Rheology of Three-Arm Asymmetric Star Polymer Melts

Amalie L. Frischknecht*,† and Scott T. Milner

ExxonMobil Research and Engineering Company, Route 22 East, Annandale, New Jersey 08801

Andrew Pryke and Ron N. Young

Department of Chemistry, University of Sheffield, Sheffield, S3 7HF, U.K.

Rhoda Hawkins and Tom C. B. McLeish

IRC in Polymer Science and Technology, Department of Physics and Astronomy, University of Leeds, Leeds, LS2 9JT, U.K.

Received January 23, 2001; Revised Manuscript Received March 15, 2002

ABSTRACT: We present experimental and theoretical results for the linear rheology of melts of entangled, three-arm asymmetric polyisoprene stars. Asymmetric three-arm stars, in which two arms have the same length and the third is shorter, cross over from starlike to linear-like stress relaxation as the length of the third arm varies. We combine recent theories of stress relaxation in symmetric stars and in linear melts to predict the dynamic modulus of the asymmetric stars. For stars with short arm molecular weights of a few entanglement lengths, our theory underestimates the effective drag caused by the short arm, even when polydispersity effects are included. This unexplained discrepancy does not appear in a recent comparison of a related theory with measurements on polyisoprene H-polymers.

1. Introduction

Entangled polymer melts can display a wide range of rheological behaviors depending on the molecular architecture. Model polymers with well-defined architectures have been crucial to advancing our understanding of polymer melt dynamics. Recently, the rheological properties of both linear and star polymer melts have been quite successfully described by tube models. In these models, polymer chains are constrained to move in a tube representing the entanglements with the other chains in the melt.[1] Linear polymers move principally by reptation, in which they diffuse curvilinearly along their confining tube.[2,3] Reptation theory predicts that the shear viscosity η_0 scales with the molecular weight M as M^3, and that the shear relaxation modulus is nearly single-exponential. The strict reptation theory assumes that the tube diameter and the contour length of the "primitive chain" representing the polymer remain constant throughout the stress relaxation. For quantitative agreement with the experimental result $\eta_0 \sim M^{3.4}$, other stress relaxation mechanisms must be included in the theory. These include contour-length fluctuations and constraint-release effects, in which the motion of surrounding chains allows transverse motion of the tube.

These mechanisms are crucial for the dynamics of star polymers. Symmetric star polymers can also be described by a tube theory, but they cannot reptate because of their central branch point. Instead, star polymers renew their configurations and thus relax stress by contour-length fluctuations of the arms. Thermal fluctuations allow the star arms to retract some distance down the confining tube toward the central branch point and then to emerge again into the entanglement network in a different configuration. Arm retractions are not favored entropically, so that deep retractions toward the center are exponentially unlikely. This leads to a wide spectrum of relaxation times in the shear relaxation modulus, with the terminal time and zero-shear viscosity both depending exponentially on the arm molecular weight M_a.

In star polymer melts, constraint-release effects are also crucial for quantitative comparisons with experiment. These effects are well-described by dynamic dilution,[4] in which the star arms in the melt see an increasingly diluted entanglement network due to the release of constraints as arms relax. A recent theory of stress relaxation with dynamic dilution in star polymer melts[5] only depends on two parameters, the plateau modulus G_N^0 and a monomeric friction factor ζ. These parameters are obtainable from data on linear melts, so in this sense the star theory is parameter free. The theory has been found to be in quantitative agreement with experiment for a wide range of star arm lengths.[5,6]

The theory for stars can also be applied to describe contour-length fluctuations in linear polymers, by treating the linear chains as two-armed stars.[7] Combined with the usual Doi−Edwards relaxation modulus, the theory correctly predicts a zero-shear viscosity $\eta_0 \sim M^{3.4}$ and produces storage and loss moduli in good agreement with experiment.

The success of these theories in describing the simplest polymer architectures gives some hope that we might now be able to understand the dynamics of melts with more complicated architectures. Of particular interest to industry would be an understanding of the behavior of lightly branched polymer melts. As steps in this direction, the theory has been recently extended to successfully describe star−star[8] and star−linear blends,[9] as well as melts of H-shaped polymers,[10] which have two branch points per molecule, and melts of comb-shaped polymers.[11]

Asymmetric star polymers, in which the arms do not all have the same lengths, are another departure from the simplest architectures of linear or symmetric star

† Present address: Sandia National Laboratories, Albuquerque, NM 87185-1349. E-mail: alfrisc@sandia.gov.

10.1021/ma0101411 CCC: $22.00
Published on Web 05/02/2002

polymers. In this paper, we investigate the simplest member of this class of polymers, namely three-arm asymmetric stars in which two of the arms have the same length and the third arm is shorter. We have seen that linear and star polymers display quite different rheological properties due to the different microscopic mechanisms of motion involved, namely reptation in the linear chains and arm retraction with dynamic dilution in the stars. One might expect that asymmetric three-arm stars, in which one arm is shorter than the other two, can cross over between these two mechanisms as the length of the third arm is varied.

For asymmetric stars, the short arm has a much shorter terminal time than the long arms, due to the exponential arm length dependence of the retraction time. Thus, once all the short arms have fully retracted to the branch points, they have relaxed all their stress and are no longer effective at entangling with the remaining unrelaxed portions of the long arms. The asymmetric star then looks like a linear chain composed of the two long arms, and the star can thus reptate. The short arm can markedly increase the drag on the remaining two arms as they reptate. As the short arm length approaches that of the long arms, a smaller fraction of the long arms is left to relax by reptation after the short arm relaxation time, so that a larger fraction of the entire star relaxes by arm retraction. We thus expect the terminal times of the asymmetric stars to lie between the terminal times for a symmetric star and a linear polymer of the same arm length. The shape of the relaxation modulus $G(t)$ should also vary between the two limits of linear-like and starlike behavior.

This crossover in the dynamics was in fact seen in a study of a series of three-arm asymmetric stars of poly(ethylene-*alt*-propylene) (PEP) by Gell et al.[12] In that study, the two long arms on each star had approximately the same molecular weights M_l for the entire series, whereas the third, shorter arm varied in molecular weight from $M_s = 0$ for the linear architecture up to $M_s = M_l$ for the symmetric star. The relaxation spectrum crossed over smoothly from the narrow spectrum of linear polymers to the broad spectrum of star polymers as the third short arm length M_s varied.

Surprisingly, the crossover to starlike behavior occurred for very short arms, by $M_s \approx 2.4M_e$ (where M_e is the entanglement molecular weight). A similar rapid crossover to starlike behavior was seen in the viscosity and self-diffusion measurements for the series. However, the PEP measurements are not optimal for comparison with the theory for two reasons. First, the molecular weight of the long arms in each star did vary across the series. Second, although it was possible to time−temperature superpose the data to create master curves for each star in the series, the temperature dependence of both the modulus and frequency shift factors varied for each star. Oddly, the result was that the onset of the Rouse regime in the loss modulus at high frequencies ($G''(\omega) \sim \omega^{1/2}$) occurred at different frequencies for different samples, which leads to ambiguities in the theoretical fits to the data.

The only other study, to our knowledge, of the dynamics of asymmetric stars was a study of tracer diffusion of a series of deuterated polybutadiene (PBD) asymmetric stars in a matrix of linear hydrogenated PBD.[13] In this case as well, the crossover to slow, starlike dynamics occurred for asymmetric stars with third arms as short as an entanglement length.

To further investigate the behavior of asymmetric stars and to compare with theory, we synthesized a series of three-arm asymmetric polyisoprene (PI) stars. Time−temperature superposition is obeyed well in PI stars. Also, PI has a low glass transition temperature, so that the high frequency regime is experimentally accessible even for large molecular weights. Finally, the entanglement molecular weight of PI is sufficiently low, on the order of $M_e = 5000$, to allow PI stars with a large degree of entanglement to be synthesized with reasonable molecular weights.

In section 2, we derive the tube model theory of stress relaxation for asymmetric stars, as an extension of the theories for relaxation in symmetric stars and for relaxation with contour-length fluctuations in linear melts. In section 3, we describe the synthesis, characterization, and rheology measurements of the PI stars. We compare the theoretical predictions with the measurements and discuss the results in the context of previous work on H-shaped polymers in section 4, and then conclude in section 5. Technical details of the calculations may be found in the appendices.

2. Tube Model Theory

In this section, we calculate the dynamic shear modulus $G^*(\omega)$ for a melt of asymmetric stars. The star arms are constrained by a tube of diameter a, which is related to the entanglement length N_e by $a^2 = 4N_eb^2/5$ (b is the statistical segment length). The modulus consists of contributions from the various types of motion undergone by the asymmetric star on different time scales. Because the relaxation time of a star arm is exponential in the length of the arm, the time scales involved are widely separated. We thus consider a hierarchy of time scales for the stress relaxation.

(i) At very early times, before the Rouse time of an entanglement segment τ_e, all the star arms undergo free Rouse motion.

(ii) After a time τ_e, the star arms "notice" that they are confined in tubes, and are no longer able to make transverse motions. Instead, the star arms renew configurations and relax stress by thermal fluctuations which allow them to retract along their tubes some distance and then poke out again into the melt in some new configuration. This regime is described by the theory for symmetric stars,[5] which gives the time $\tau(s)$ for a star arm to retract a fractional distance s ($0 \le s \le 1$) from the free end of its tube. The entanglement network dynamically dilutes as the arms retract and release constraints on other arms. The long arms retract more slowly than the short arms, so there are two arm retraction times, $\tau_l(s_l)$ for retractions a fractional distance s_l along a long arm, and $\tau_s(s_s)$ for retractions a fractional distance s_s along the short arm.

(iii) The short arm will have fully retracted when $s_s = 1$, at time $\tau_s^* \equiv \tau_s(s_s = 1)$. At this time, the short arms have completely relaxed and are thus no longer effective at entangling with the long arms.

(iv) After τ_s^*, the long arms continue to retract, in a still-diluting entanglement network which no longer includes any contribution from the short arms.

(v) Eventually, the remaining two long arms will be able to relax stress more quickly by reptation than by arm retraction. The third short arm acts as extra drag on the effective linear chain formed by the two long arms. Thus, the "backbone" consisting of the two long arms will relax by reptation after the retraction time

of the long arms becomes equal to the reptation time τ_d of the backbone:

$$\tau_l(s_d) \equiv \tau_d \tag{1}$$

This equation defines the quantity s_d, which is the fractional distance the long arms have retracted down their tubes at time τ_d. After this time, the rest of the stars relax by reptation.

We begin by outlining the calculation of the arm retraction times from the theory for symmetric stars[5] (details are given in Appendix A). There are two regimes in the retraction of an arm. For sufficiently large displacements s down the tube, the retraction is entropically unfavorable, since the star arm must form unentangled loops inside the tube or emerging from its sides in order to retract. Pearson and Helfand calculated the free energy cost for arm retraction in a fixed network to be $U(s) = \nu(N_a/N_e)s^2$ (in units of k_BT), where $\nu = 15/8$.[14] For large N_a/N_e the barrier is many times k_BT, so arm retraction is an activated process and $\tau(s) \sim \exp[U(s)]$. The exponential dependence of $\tau(s)$ on s^2 and on N_a/N_e leads to a broad range of relaxation times along the star arm. In a melt of stars, this means that on a time scale $\tau(s)$, segments a distance $s' < s$ from the free end have long since relaxed and are no longer effective at entangling with segments at s. The fraction of the star arms which are unrelaxed at time $\tau(s)$ thus see an entanglement network which has been diluted by the removal of the faster-moving, relaxed arm segments. The entanglement length at $\tau(s)$ depends on the volume fraction of unrelaxed segments $\Phi(s) = 1 - s$ as

$$N_e(\Phi) = N_e/\Phi^\alpha, \quad N_e(s) = N_e/(1-s)^\alpha \tag{2}$$

A scaling argument of Colby and Rubinstein[15] as well as experiments on the concentration of the plateau modulus in Θ solutions imply that $\alpha = {}^4/_3$, which we use here. The dynamic dilution of the arms in the melt leads to a renormalization of the potential $U(s)$ for arm retraction to a new effective potential $U_{eff}(s)$, which is the solution to a differential equation given by Ball and McLeish:[4]

$$\frac{d}{ds}\ln\tau(s) = \frac{\partial U}{\partial s}(s; N_e(s)) \equiv \frac{dU_{eff}}{ds}(s) \tag{3}$$

For asymmetric stars, the effective potential $U_{eff}(s)$ for activated arm retractions is different for long and short arms. Applying the Ball−McLeish eq 3 for the retraction time of an arm with $n_i = N_i/N_e$ entanglement segments, we find

$$\frac{d(\ln\tau_i)}{ds_i} = 2\nu n_i s_i \Phi^\alpha \tag{4}$$

where s_i is the fractional distance retracted down the tube of arm i. The unrelaxed volume fraction of chains Φ at time $\tau_i(s_i)$ is

$$\Phi = \begin{cases} \phi_s(1-s_s) + \phi_l(1-s_l), & s_s < 1, \tau < \tau_s^* \\ \phi_l(1-s_l), & \tau > \tau_s^* \end{cases} \tag{5}$$

where ϕ_s (ϕ_l) is the overall volume fraction of short (long) arms. We see immediately from eq 4 that the short and long arms retract at different rates. We can eliminate all dependence on the different arm lengths in eq 4 by making a change of variables to $y = n_i s_i^2$.[8] Rewriting eq 4 we have

$$\frac{d(\ln\tau)}{dy} = \nu\Phi^\alpha = \frac{dU_{eff}(y)}{dy} \tag{6}$$

which now holds for both arms. Thus, it takes the same amount of time for either a long or a short arm to retract from $y = 0$ to a given value of y. We can now write Φ as a function of the single variable y, noting that $y = n_s$ when the short arm has fully retracted to $s_s = 1$:

$$\Phi(y) = \begin{cases} \phi_s(1-\sqrt{y/n_s}) + \phi_l(1-\sqrt{y/n_l}), & y < n_s \\ \phi_l(1-\sqrt{y/n_l}), & y > n_s \end{cases} \tag{7}$$

The change of variables from the coordinates s_s and s_l along the tubes to y allows us to calculate the effective potentials for the short and long arms by solving eq 6 for $\tau(y)$, using eq 7.

The activated retraction time $\tau_a(s)$ for an arm to retract a distance s in its effective potential U_{eff} is then $\tau_a(s) \propto \exp[U_{eff}(s)]$. The prefactor can be calculated quantitatively by solving a first-passage time problem. The general result is[5]

$$\tau_a(s) = (L^2/D_{eff})\int_0^s ds' \exp[U_{eff}(s')]\int_{-\infty}^{s'} ds'' \exp[-U_{eff}(s'')] \tag{8}$$

where L is the contour length and D_{eff} is the effective curvilinear diffusion constant of the retracting arm in its tube. The contour length for an arm of length N_a is $L = N_a b^2/a = 5/4(N_a/N_e)a$. In ref 5, it was argued that the effective diffusion constant for arm retraction should be twice the Rouse diffusion constant, $D_{eff} = 2D_R = 2k_BT/(N_a\zeta)$, where ζ is the monomeric friction factor.[5] The full expressions for the arm retraction times $\tau_{a,i}(s)$ in the activated regime are given in Appendix A. They depend explicitly on both the lengths and on the volume fractions of the short and long arms. Essentially, in the limit where the third arm is quite short, the long arms are mostly immobile while the short arm is retracting so that it mostly sees a fixed entanglement network with only a small amount of dilution. As the third arm becomes longer, more of the entanglement network dilutes while it retracts, due both to retractions of the other short arms and to more extensive retractions of the long arms. Thus, the nature of the entanglement network during the arm retractions depends explicitly on the volume fractions of the long and short arms.

For very early times, the entropic barrier to retraction is less than k_BT, $U_{eff} < k_BT$. Then the effective potential is unimportant, and the arm free end diffuses freely by Rouse motion in the tube. The mean-square displacement of any monomer on a Rouse chain in a tube, including the free end, scales as $s^2 \sim t^{1/2}$. On inversion this gives the relaxation time $\tau_{early}(s)$ in the small s or early time regime:[5]

$$\tau_{early}(s) = (225\pi^3/256)\tau_e s^4 (N/N_e)^4, \tag{9}$$

where $\tau_e = \zeta N_e^2 b^2/(3\pi^2 k_BT)$ is the Rouse time of an entanglement segment of length N_e and the prefactor in eq 9 is fixed by an explicit Rouse calculation. Both long and short arms will exhibit the same short time fluctuations near their free ends. Complete arm retraction times, over the entire range of arm retraction, are

constructed by combining the activated (eqs A14 and A15) and early time results (eq 9) for each arm using a crossover function:[6]

$$\tau_i(s_i) = \frac{\tau_{\text{early}}(s_i)\,\exp[U_{\text{eff},i}(s_i)]}{1 + \exp[U_{\text{eff},i}(s_i)]\tau_{\text{early}}(s_i)/\tau_{\text{a},i}(s_i)} \tag{10}$$

Next we need to calculate the reptation time τ_d of the two long arms. The short arm can be thought of as causing extra drag by decreasing the curvilinear diffusion constant of the "linear" backbone formed by the two long arms. The branch point of the star can only make a diffusive hop along the tube of the backbone about once every short arm retraction time τ_s^*, when the short arm has retracted all the way to the branch point and is unentangled. Each time the short arm is retracted, the branch point is free to move a distance of about a tube diameter. One might expect the branch point to hop a distance of order the dilated tube diameter; however, a recent comparison of the theory with self-diffusion data on symmetric star melts indicates that the branch point only hops a distance of order the undiluted tube diameter given by $a^2 = (4/5)N_e b^2$.[16] We will consider both possibilities here.

Thus, the effective curvilinear diffusion constant of the branch point along the tube of the backbone can be written as

$$D_b = \frac{(pa_h)^2}{2\tau^*_s} \tag{11}$$

where a_h is equal to either the undiluted tube diameter a or the dilated tube diameter a_d. The mean hopping distance of the branch point after a time τ_s^* could be some fraction of a tube diameter, so in eq 11 the branch point is assumed to hop a distance pa_h, where we expect p to be a (dimensionless) constant of order unity. The total drag on the reptating backbone is found by adding the effective drag caused by the short arm to the drag from the monomeric friction along the backbone. Since the drag is inversely proportional to the diffusion constant, the net curvilinear diffusion constant of the long arms is

$$1/D_{\text{eff}} = 1/D_b + 1/D_c \tag{12}$$

where $D_c = k_B T/2N_l\zeta$ is the Rouse diffusion constant. The short arm retraction time τ_s^* depends exponentially on n_s, so the effective drag caused by the short arm can be quite large, in general much larger than the Rouse drag. Thus, for most values of n_s, the second term in eq 12 will be negligible compared to the first.

The reptation time is the time it takes the stars to diffuse the curvilinear length of the linear backbone. Only a fraction $1 - s_d$ of the long arms are still unrelaxed at time $\tau_d = \tau_l(s_d)$ when they start to execute reptation. The contour length of the reptating portion of the long arms is thus $L_{\text{eff}}(1 - s_d)$, where L_{eff} is the effective contour length of the backbone (of length $2n_l$). The reptation time is then[7]

$$\tau_d = \frac{L_{\text{eff}}^2(1 - s_d)^2}{\pi^2 D_{\text{eff}}} \tag{13}$$

Since the short arms have fully relaxed long before τ_d, one might expect the backbone to reptate in a dilated tube, formed only by entanglements with the other long arms. In this case, the backbone reptates in a tube of diameter a_d given by $a_d^2 = (4/5)N_e b^2/\phi_l^\alpha = a^2/\phi_l^\alpha$ and thus consists of entanglement segments of length N_e/ϕ_l^α. Substituting $L_{\text{eff}}/a_{\text{eff}} = (5/4)(2n_l)/\phi_l^\alpha$ in eq 13 and using eqs 11 and 12, we have for the reptation (disentanglement) time in a dilated tube:

$$\tau_{d,d} = \begin{cases} \dfrac{15}{4}(2n_l)^3\tau_e(1 - s_d)^2\phi_l^\alpha\left(1 + \dfrac{5}{6\pi^2 p^2 2n_l}\dfrac{\tau_s^*}{\tau_e}\right), & a_h = a \\ \dfrac{15}{4}(2n_l)^3\tau_e(1 - s_d)^2\phi_l^\alpha\left(1 + \dfrac{5}{6\pi^2 p^2 2n_l}\dfrac{\tau_s^*\,\phi_1^\alpha}{\tau_e}\right), & a_h = a_d \end{cases} \tag{14}$$

where the first form assumes the branch point hops in a "skinny tube" of diameter a, and the second assumes that it hops in a dilated tube. On the other hand, if both the branch point hops and the backbone reptation occur in an undilated skinny tube of diameter a, there is no explicit dependence on ϕ_l in τ_d:

$$\tau_d = \frac{15}{4}(2n_l)^3\tau_e(1 - s_d)^2\left(1 + \frac{5}{6\pi^2 p^2 2n_l}\frac{\tau_s^*}{\tau_e}\right) \tag{15}$$

In all three expressions for τ_d, the factor of 1 in the parentheses is the Rouse contribution to the drag. The second term in parentheses is the effect of the extra drag due to the third arm. Together with eq 1, eq 14 (or eq 15) defines the reptation time and gives an implicit equation for s_d.

We can now calculate the dynamic modulus using the expressions for the various time scales involved. The portion of the stress relaxing due to the arm retractions is found generally from summing the contributions relaxing at each time τ:

$$G(t) = -\int_0^{\tau_d} d\tau \frac{\partial G}{\partial \Phi}\frac{\partial \Phi}{\partial \tau} e^{-t/\tau} \tag{16}$$

The concentration dependence of the modulus is $G(\Phi) = G_N^0\Phi^{1+\alpha}$, where G_N^0 is the plateau modulus. Summing the contributions of the long and short arms, changing variables in the integration from τ to s, and taking the Fourier transform of eq 16, we have

$$G^*_{\text{retract}}(\omega) = G_N^0(1 + \alpha)\left[\phi_s\int_0^1 ds_s(1 - g_s s_s)^\alpha \frac{i\omega\tau_s(s_s)}{1 + i\omega\tau_s(s_s)} + \phi_l\int_0^{s_l^*} ds_l(1 - g_l s_l)^\alpha \frac{i\omega\tau_l(s_l)}{1 + i\omega\tau_l(s_l)} + \phi_l^{\alpha+1}\int_{s_l^*}^{s_d} ds_l(1 - s_l)^\alpha \frac{i\omega\tau_l(s_l)}{1 + i\omega\tau_l(s_l)}\right] \tag{17}$$

where the g_i are constants defined in Appendix A, and s_l^* is the fractional distance the long arms have retracted at the short arm retraction time, defined by $\tau_l(s_l^*) = \tau_s^*$. After the reptation time, the backbone relaxes with the Doi–Edwards spectrum,[3] with the modification that only a fraction $G[\Phi(s_d)]/G_N^0 = [\phi_l(1 - s_d)]^{1+\alpha}$ of the stress remains to be relaxed:[7]

$$G^*_{\text{reptate}}(\omega) = G^0_N[\phi_l(1 - s_d)]^{1+\alpha} \sum_{p\ \text{odd}} \frac{8}{\pi^2 p^2} \frac{i\omega\tau_d}{p^2 + i\omega\tau_d} \quad (18)$$

Finally, we include the stress relaxation due to Rouse modes at short times, following ref 7. The Rouse stress relaxation function is

$$G_{\text{Rouse}}(t) = G^0_N(N_e/N) \sum_{p=1}^{N} \exp[-p^2 t/\tau_R] \quad (19)$$

where $\tau_R = (N/N_e)^2\tau_e$ is the Rouse relaxation time. Equation 19 is essentially independent of chain length for $t < \tau_R$. Furthermore, for times less than the Rouse time of an entanglement segment τ_e, all segments in the star execute free Rouse motion so eq 19 holds for the entire star. On time scales longer than τ_e, the arms notice that they are confined to tubes and only longitudinal Rouse modes are possible. We include these by multiplying the low-frequency contribution (with modes $1 \le p \le N/N_e$) of eq 19 by $^1/_3$. Weighting the results by the volume fractions of the short and long arms we have

$$G^*_{\text{Rouse}}(\omega) = \phi_s G^*_{\text{Rouse}}(\omega, N_s) + \phi_l G^*_{\text{Rouse}}(\omega, N_l) \quad (20)$$

where

$$G^*_{\text{Rouse}}(\omega, N_i) = \frac{G^0_N}{3n_i} \sum_{p=1}^{n_i} \frac{i\omega\tau_e {n_i}^2/p^2}{1 + i\omega\tau_e {n_i}^2/p^2} + \frac{G^0_N}{n_i} \sum_{p=n_i+1}^{N_i} \frac{i\omega\tau_e {n_i}^2/p^2}{1 + i\omega\tau_e {n_i}^2/p^2} \quad (21)$$

The full modulus for the asymmetric star is the summation of the contributions from arm retractions, reptation, and the early time Rouse modes:

$$G^*(\omega) = G^*_{\text{retract}}(\omega) + G^*_{\text{reptate}}(\omega) + G^*_{\text{Rouse}}(\omega) \quad (22)$$

The dynamic modulus depends on two parameters, the plateau modulus G^0_N and the monomeric friction factor ζ through τ_e. The entanglement molecular weight is related to G^0_N by $G^0_N = \rho RT/M_e$, where ρ is the density of the polymer melt. There is also a third unknown (possibly universal?) parameter in the theory that is particular to branched polymers, namely the dimensionless factor p in eq 11 for the effective diffusion constant of the branch point.

3. Experiments

Synthesis. A series of polyisoprene star samples was synthesized in which two of the arms had an approximately constant weight (105 000 g mol^{-1}) and the third arm varied in molecular weight from 0 (i.e., a linear material) to about 105 000 g mol^{-1} (i.e., a symmetric star). The samples will be referred to as ss105 for the symmetric star, as l210 for the linear material, and as as47, as37, as17, and as11 for the asymmetric stars with short arm molecular weights of approximately 47 000, 37 000, 17 000, and 11 000 g/mol, respectively.

All the polymer samples were prepared using well-established anionic techniques[17] under high vacuum conditions. All polymerizations were carried out in degassed *n*-hexane, which had been purified by stirring over sodium/potassium alloy for 24 h followed by distillation from *n*-butyllithium. Isoprene monomer was purified by stirring over dibutylmagnesium for 24 h prior to distillation to the reaction vessel. The chosen initiator, *s*-butyllithium (*s*-BuLi), was distilled under high vacuum in a short path length apparatus and diluted with *n*-hexane. Quantities of solution were then measured into ampules equipped with dome-type break-seals via a vacuum buret apparatus. The concentration of the dilute solution was determined by titration. Methyl trichlorosilane ($MeSiCl_3$), used to link three arms together to form stars, was purified by distillation directly into ampules such that each contained approximately 1 mL.

Polybutadienyllithium was prepared in *n*-hexane using *s*-BuLi as initiator, the reaction being allowed to proceed for 24 h to ensure complete polymerization. Living polymer destined to form the short arm was reacted with the contents of an $MeSiCl_3$ ampule, which were added to the solution with good agitation. A nearly 100-fold molar excess of $MeSiCl_3$ in relation to the chain ends present was employed to ensure that there was a minimal possibility of more than one living chain end becoming attached to any silicon atom. After stirring at ambient temperature for 24−48 h, the majority of the unreacted chlorosilane was removed by vacuum distillation. Final traces of $MeSiCl_3$ were removed by redissolving the polymer in fresh *n*-hexane and redistilling under vacuum, a process that was repeated to ensure that no linking reagent remained. Once redissolved in *n*-hexane, a sample of the functionalized arms was isolated in a small subsidiary vessel equipped with a greaseless stopcock for GPC analysis.

The polybutadienyllithium intended to form the two long arms of a star was synthesized in a separate vessel, again in *n*-hexane at ambient temperature. The quantity of these arms employed was in a small excess over the necessary stoichiometry, such that upon addition to the functionalized short arms only three-armed star and long arms remained at the end of the reaction, thus making for easier purification by fractionation. The vessels containing the living long arms and the functionalized short arms were then linked via short attachments equipped with dome-type break-seals, one of which had a Quickfit socket for attachment to the vacuum line enabling evacuation of the center section. A schematic representation of a typical setup is shown in Figure 1.

Once joined, the center section was evacuated and the reactors removed from the vacuum line by sealing the constriction; both break-seals were broken and the contents of the two reactors mixed well by pouring back and forth between the vessels. The mixture was then stirred at ambient temperature for 5−7 days after which any remaining living arms were terminated via the addition of degassed methanol. Polymer was recovered by precipitation in methanol to which a small quantity of antioxidant had been added. Small samples of each polymer were then taken for GPC analysis. Typical GPC results from such an asymmetric star synthesis are illustrated in Figure 2.

To complete the series two more samples were prepared, a symmetric star and a linear polymer with a molecular weight twice that of the long arms used throughout the series, i.e., a "two-armed" star. The symmetric star was produced by linking a batch of living arms with a slightly less than stoichiometric quantity of $MeSiCl_3$, while the "two-armed" linear material was synthesized by terminating a batch of linear polyisoprene of the appropriate molecular weight.

The crude star polymers were purified by repeated fractionation from a toluene/methanol solvent/nonsolvent system. In most cases 2−3 fractionations were sufficient to yield a product, which when analyzed via GPC revealed no more than 1% remaining low molecular weight material by integrated peak areas. Selected GPC data collected during fractionation is shown in Figure 3.

Molecular weights of the arms were measured by GPC. The molecular weight of the assembled stars were likewise measured by GPC and in several cases by light scattering (LS) using a triple-detector GPC analysis and d*n*/d*c* values from the literature for linear 1,4-PI. The results are tabulated in Table 1. LS determines the chain mass from the amplitude of forward scattering and is thus insensitive to chain architec-

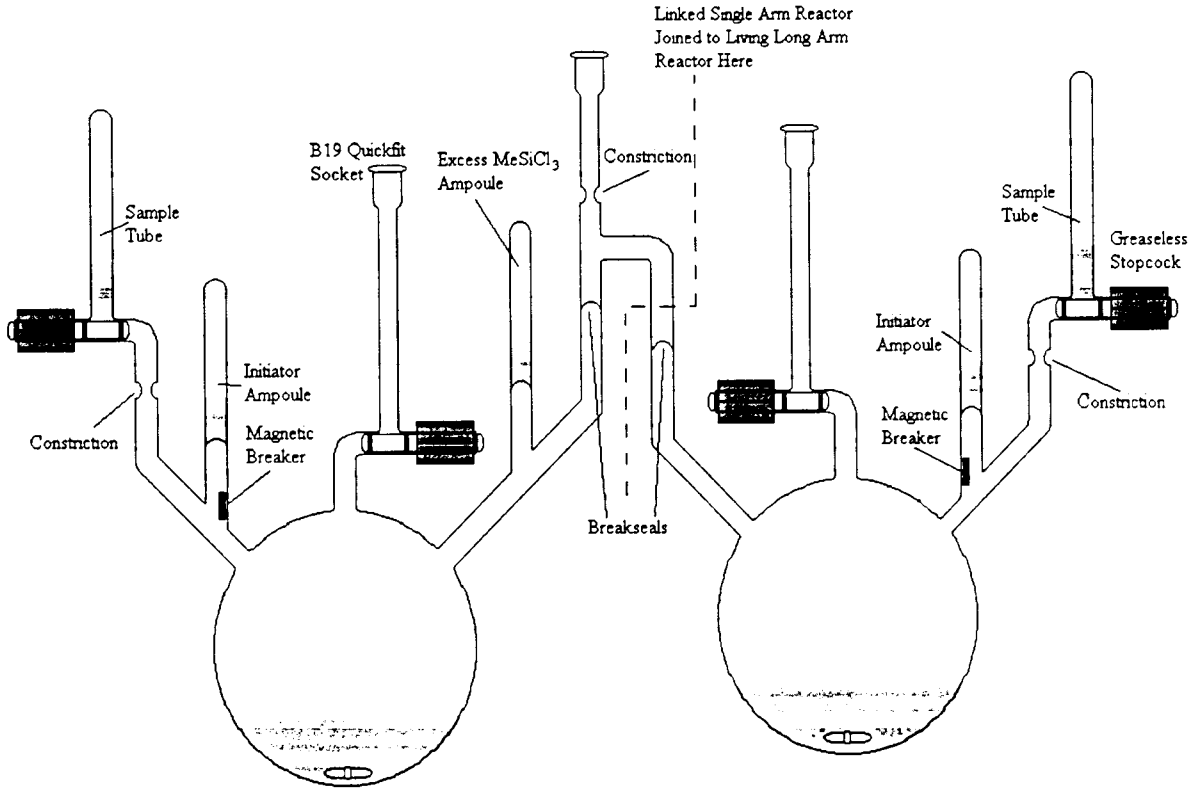

Figure 1. Typical asymmetric star reactor configuration.

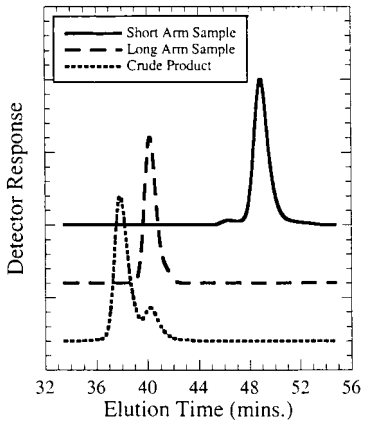

Figure 2. GPC analyses of samples taken during the course of the synthesis of the asymmetric polyisoprene star sample as11.

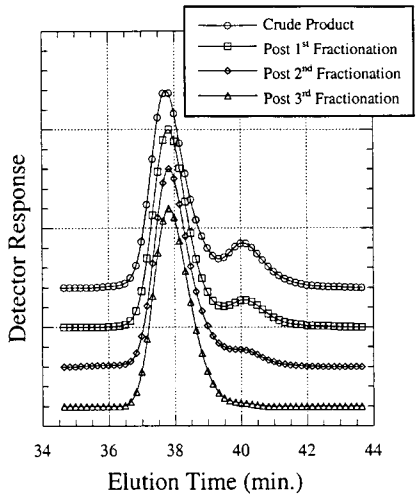

Figure 3. GPC analysis of the asymmetric star as11 after three sequential fractionations.

ture. In contrast, GPC essentially provides a measure of the hydrodynamic size of the polymers, as chains of larger coil dimension avoid small nooks and crannies in the GPC column and thus pass through more quickly. Molecular weights are calibrated by comparison to a reference polymer of linear architecture. Roughly speaking, branched polymers have smaller coil dimensions that linear chains of the same mass; thus branched polymers pass through a GPC column more slowly, and are assigned a spuriously low mass. The results in column 4 of Table 1 have not been corrected for this effect.

Simple calculations (assuming ideal random-walk dimensions) suggest that for asymmetric three-arm stars, the so-called "*g* factor" (ratio of square radius of gyration to that of a linear chain of equal mass) is $g(r) = (8 + r^3 + 6r(1 + r))/(2 + r)^3$, where r is the ratio of short arm mass to long arm mass. For symmetric three-arm stars, $g = {}^7/_9 = 0.78$; for highly asymmetric stars, $g \approx (1 - 3r/4)$. If we assume the ratio of square hydrodynamic radii is similar to the ratio of R_g^2, then the naively inferred star masses from GPC in Table 1 should be multiplied by $1/g(r)$. Making this correction would increase the value of the star masses inferred by GPC to 215K, 218K, 275K, 244K, and 346K, which are reasonably consistent with the sum of the arm masses measured by GPC (225K, 251K, 253K, 270K, and 312K; see colunm 5 of Table 1). These values are also consistent with the available results for star mass measured by LS, with the exception of the symmetric star for which the LS value is clearly too low relative to the GPC results.

As we shall see below, the extreme sensitivity of the rheological results to the arm lengths provides a strong check of values of these molecular weights, and in the case of the symmetric star, it compels us to adjust slightly the arm length we assume.

The microstructure of the polymers was established using ^{1}H NMR analysis,[18] employing the relative integrals of the peaks present at 1.69, 1.65, 1.74, 4.81, and 5.24 ppm. Values were, as expected, nearly constant throughout the series with

Table 1. Molecular Characterization

architecture and expected arm mol wt (kg mol^{-1})	long arm mol wt by (1) GPC (2) LS (g mol^{-1})	short arm mol wt by (1) GPC (2) LS (g mol^{-1})	star mol wt (1) GPC[a] (2) LS (g mol^{-1})	star mol wt (1) corrected GPC (2) sum of arm weights	star polydispersity by GPC	% microstructure by ^{1}H NMR (1) *cis*-1,4 (2) *trans*-1,4 (3) 3,4
linear 210	N/A	N/A	(1) 212 000 (2) 224 000	N/A	1.02	
asymmetric star 105-105-11	(1) 107 000	(1) 11 500	(1) 201 000 (2) 215 000	(1) 215 000 (2) 225 000	1.02	(1) 78.2 (2) 15.8 (3) 6.0
asymmetric star 105-105-17	(1) 116 000	(1) 19 000	(1) 197 000	(1) 218 000 (2) 251 000	1.01	
asymmetric star 105-105-37	(1) 107 000	(1) 39 000	(1) 230 000	(1) 275 000 (2) 253 000	1.01	(1) 80.2 (2) 15.0 (3) 4.8
asymmetric star 105-105-47	(1) 117 000 (2) 110 000	(1) 36 500 (2) 40 000	(1) 207 000	(1) 244 000 (2) 270 000	1.02	
symmetric star 105-105-105	(1) 104 000	N/A	(1) 269 000 (2) 261 000	(1) 346 000 (2) 312 000	1.01	

[a] Raw star molecular weights calculated using identical calibration factors to those employed for linear samples; see text for discussion.

78−80% *cis*-1,4, 15−17% *trans*-1,4, 4−6% 3,4, and negligible 1,2. The characterization results are given in Table 1.

Rheology. Linear rheological spectra were obtained in oscillatory shear between parallel plates. Data from two machines, a Rheometrics RDA II and RDS, were combined. Samples were first formed into 25 mm diameter disks with typical thicknesses of between 0.5 and 1.5 mm. Temperatures from −60 to +120 °C were used to cover an effective frequency range 10^{-4}−10^{7} rad s^{-1} at 25 °C by time−temperature superposition. All strains were measured to be in the range of linear response. In all cases the terminal zone was reached. Repeated measurements after runs at the highest temperatures did not detect any significant degradation. Carrying out the rheology under a nitrogen atmosphere and in the presence of added antioxidant helped to ensure sample stability.

Data sets collected at different temperatures were time−temperature superposed to 25 °C by manually shifting each data set, plotting the resultant values of log a_T against $T - T_0$ and fitting a curve of the form

$$\log a_t = \frac{-C_1(T - T_0)}{C_2 + T - T_0}$$

to the points in order to derive C_1 and C_2. The fit gave the WLF factors $C_1 = 5.0$ and $C_2 = 140$, which were applied to rheology data collected for all the polymers in the series. Previous work on linear polyisoprene obtained similar values of $C_1 = 4.1$ and $C_2 = 122$.[19]

4. Results and Discussion

The rheology data for the entire series for $G'(\omega)$ and $G''(\omega)$ at a reference temperature of 25 °C is shown in Figures 4 and 5. The entire range of viscoelastic behavior is represented in the data, except for the terminal region in $G'(\omega)$ for some of the samples. The data from all the samples overlap in the high-frequency Rouse regime, which is independent of architecture and molecular weight. As expected, the linear polymer has the shortest terminal time and the symmetric star polymer the longest, with the terminal times of the asymmetric stars falling in between in order of the short arm molecular weight. We note that the loss modulus of all the asymmetric stars has the broad shape characteristic of star polymers; even sample as11, with a short arm consisting of a couple of entanglement lengths, has a spectrum that looks more like that of a star polymer than that of a linear polymer.

As discussed in section 2, the theory depends on only two independent parameters: the Rouse time of an entanglement segment τ_e, and the plateau modulus G_N^0 (or the entanglement molecular weight M_e). These parameters can be obtained by fitting the data either for the symmetric star or for the linear chain to the

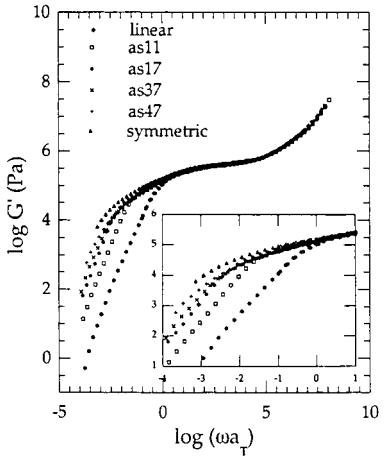

Figure 4. Overlayed storage modulus plots obtained from linear, asymmetric and symmetric polyisoprene star samples. Samples l210 (circles), as11 (open squares), as17 (diamonds), as37 (crosses), as47 (pluses), and ss105 (open triangles). The inset shows the terminal region in more detail.

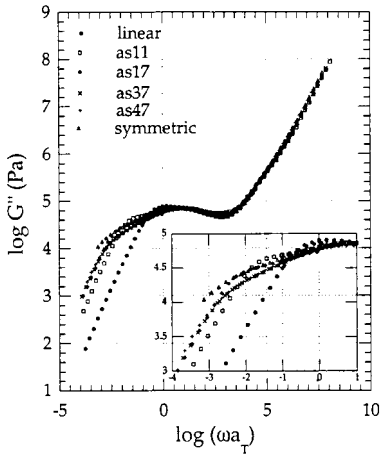

Figure 5. Overlayed loss modulus plots obtained from linear, asymmetric and symmetric polyisoprene star samples. Samples l210 (circles), as11 (open squares), as17 (diamonds), as37 (crosses), as47 (pluses), and ss105 (open triangles). The inset shows the terminal region in more detail.

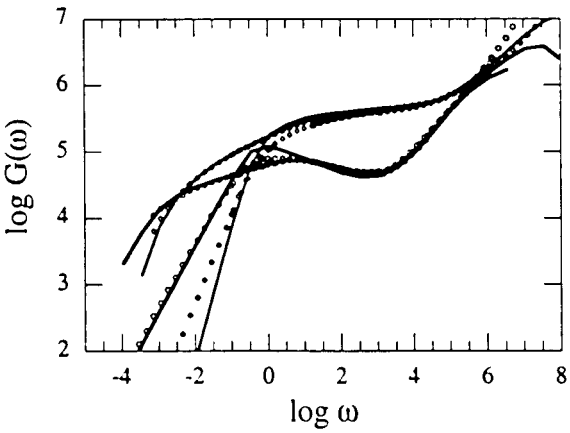

Figure 6. Data and theoretical predictions of $G'(\omega)$ (diamonds) and $G''(\omega)$ (circles) for the symmetric star (open symbols) and the linear chain (filled symbols).

appropriate versions of the theory, noting that the values should be comparable to values from the literature for 1,4-PI. Other than the dimensionless constant p in eq 11, this then allows us to do a parameter-free fit to the asymmetric star data.

We thus first fit the data for the symmetric star and the linear chain. The value of τ_e can be found unambiguously by requiring that the theoretically predicted curves overlap the data in the high-frequency Rouse regime (adjusted by shifting the theory curve along the frequency axis). The value of the plateau modulus is extracted by ensuring that the theory overlays the data in the vertical direction. The entanglement molecular weight is then given by $M_e = \rho RT/G_N^0$. Using this procedure, we find that the best fit parameters are

$$\tau_e = 8.9 \times 10^{-6}\ \text{s}$$

$$G_N^0 = 0.49\ \text{MPa}, \quad M_e = 4551\ \text{g/mol} \qquad (23)$$

where we have used $\rho = 0.9$ g/cm^3 for 1,4-PI,[20] in calculating M_e from G_N^0. With this value of M_e, the length of the linear chain is $n_{lin} = M_{lin}/M_e = 24.6$ (where n_{lin} is the length of one "arm" of the linear chain, i.e., half the linear chain length, and we use the light scattering value of $M_{lin} = 224$ K which should be more accurate than the GPC value). We find that this value gives an excellent fit to the data. As we see from Table 1, the GPC measurement of the symmetric star arms is not consistent with the light scattering value for the total star molecular weight. We find the best fit to the data at about $n = 20.5$, which corresponds to a star arm molecular weight of $M_a = nM_e = 93.3$ K. This gives a total star molecular weight of $M = 279$ K, which lies between the light scattering and GPC values. The fits using these parameters are shown in Figure 6. The fit for the symmetric star data is excellent, as is the fit for the loss modulus of the linear chains. The fit for the storage modulus of the linear species is good except in the terminal region, where the data displays a small shoulder before reaching the terminal behavior of $G'(\omega) \sim \omega^2$.

The parameter values obtained from the fits are reasonably consistent with literature values for 1,4-PI. From ref 20, for 1,4-polyisoprene at 298 K the entanglement molecular weight is 5097 g/mol and $G_N^0 = 0.35$ MPa. We can also estimate τ_e from literature values. Again from ref 20, at 298 K the chain end-to-end radius squared per chain mass is $\langle R^2\rangle/M = 0.596$ Å^2 mol/g. With a monomer mass of $M_0 = 68$ g/mol, this gives $b = \sqrt{M_0\langle R^2\rangle/M} = 6.37$ Å. From Ferry, the monomeric friction factor ζ at 298 K is $\log \zeta = -6.41$ in cgs units,[21] so $\tau_e = \zeta N_e^2 b^2/(3\pi^2 k_B T) = 7.29 \times 10^{-6}$ s.

Using the values in eq 23 for the parameters, we can now fit the asymmetric star samples. We use the measured values for the arm molecular weights, using light scattering values where available and the GPC values otherwise, and keep the entanglement molecular weight fixed at $M_e = 4551$ g/mol. We note that this is a different procedure than that used in ref 10 to fit theory to the shear modulus of H-polymers. In the case of an H-polymer, there are two distinct relaxation times visible in the data (particularly in $G''(\omega)$) due to the relaxation of first the arms and then the crossbars. Since the theory is quite sensitive to the lengths of the arms, these distinguishing features in the rheology allow one to fit the lengths of the arms and crossbars separately and then compare to the measured molecular weights; this procedure allows for small discrepancies between G_N^0 and M_e, or for small uncertainties in the molecular weight determinations. This protocol was also used in previous studies of symmetric star polymers.[6] The asymmetric star data, by contrast, does not have distinct features due to relaxations of the short arms vs those of the longer arms. Thus, we are not able to make separate fits of n_s and n_l, and must instead rely upon the experimentally measured values.

We recall from section 2 that there are three possibilities for the dynamics of the branch point and the reptation. We consider each of these in turn. First we consider the slowest possible dynamics, namely that the branch point hops in a "skinny" tube and that the backbone likewise reptates in this skinny tube, of diameter a, with reptation time τ_d given by eq 15. With these assumptions, we would expect the theory to overpredict the terminal times, since dynamic dilution implies that the backbones should reptate in dilated tubes instead. Figure 7 shows the theoretical predictions for $G^*(\omega)$ for the asymmetric stars, with the unknown constant in the branch point diffusion (eq 11) set to $p = 1$. The high-frequency end of the spectrum remains the same for all the stars because the Rouse modes are not dependent on molecular weight or architecture. We see the values of τ_e and G_N^0 found in eq 23 from the linear and symmetric star samples are quite good for the asymmetric stars as well. As expected, the theory overpredicts the terminal times for samples as47 and as37. Surprisingly, however, the theory slightly underpredicts the terminal time for as17 and underpredicts it by quite a bit for sample as11.

We next try the more reasonable assumption that the backbone reptates in a dilated tube, with the branch point hopping in a skinny tube as was suggested by the results of ref 16. Employing eq 14 with $a_h = a$ in calculating $G^*(\omega)$ and again setting $p = 1$ leads to the prediction shown in Figure 8. The theory now gives a rather good fit to the data for samples as47 and as37. However, for the two samples with the shortest third arms, samples as17 and as11, the predicted terminal time is considerably shorter than the measured one. Furthermore, the predicted loss moduli for samples as11 and as17 show a distinct reptation peak, whereas the data show broad, starlike shoulders in the loss moduli. We note that the short arms throughout the series are well-entangled, with the shortest arm with a molecular

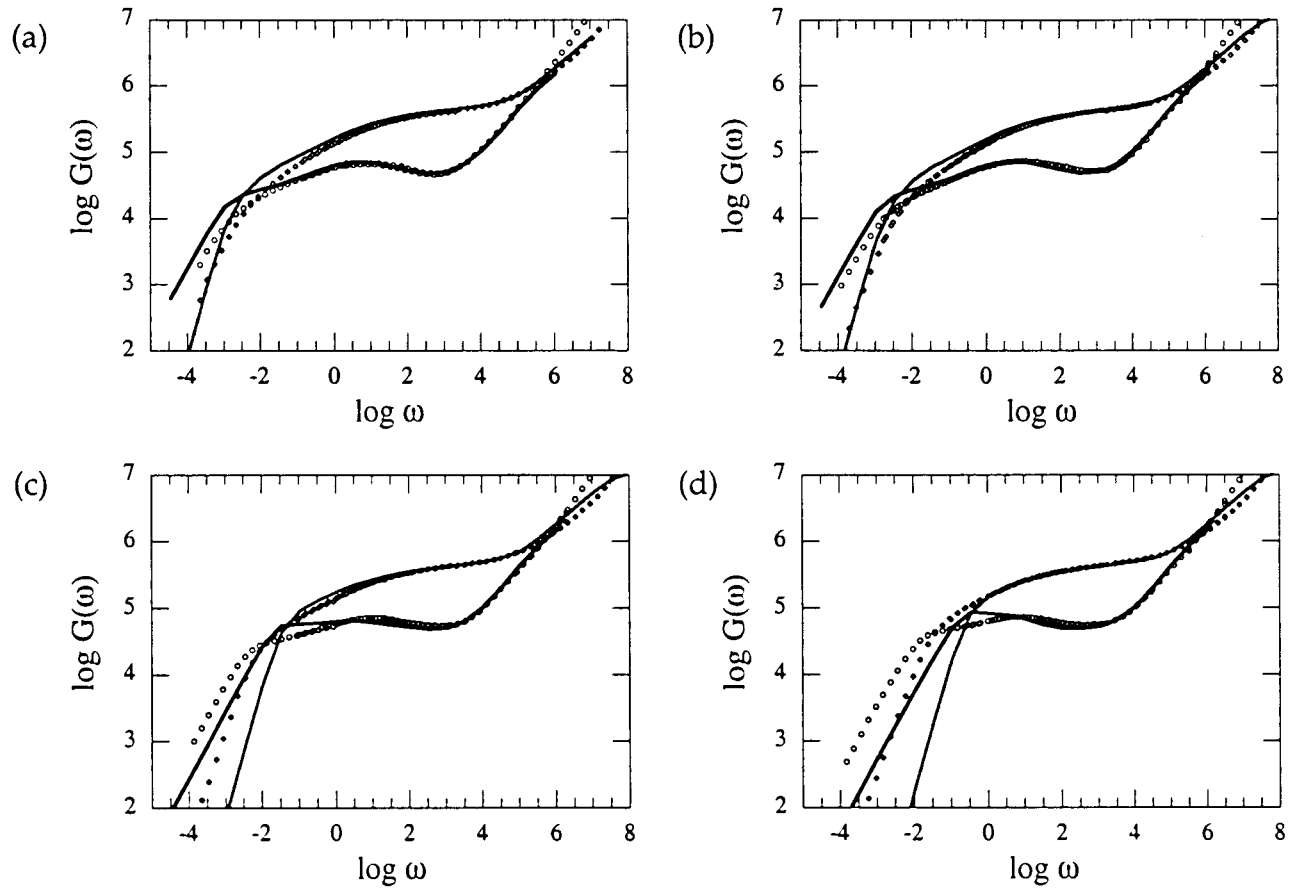

Figure 7. Reptation and hops in skinny tubes: Data and theoretical predictions of $G'(\omega)$ (diamonds) and $G''(\omega)$ (open circles) for the asymmetric stars with $p^2 = 1$: (a) as47, (b) as37, (c) as17, and (d) as11.

weight of 11.5 kg/mol consisting of about 2.5 entanglement molecular weights.

Finally, Figure 9 shows the results for both backbone reptation and branch point hopping in dilated tubes, with $p = 1$. Since these assumptions speed the relaxation even further, the theory now slightly underpredicts the terminal times for samples as47 and as37, while further worsening the fit for samples as17 and as11.

These results are quite puzzling, as we now show. The theories for the symmetric star and the linear chain fit the data quite well and have been shown to successfully describe rheology data in other polymer systems. There are only two new elements in the theory for the asymmetric stars. The first is the calculation of the arm retraction times, incorporating dynamic dilution, in a melt of arms of varying lengths. Similar calculations were carried out in studies of star−star blends[8] and were found to agree well with experiment. Furthermore, the success of the physical picture of dynamic dilution in describing the arm relaxation makes it unlikely that this is the source of the discrepancies.

The second new element in the theory is the calculation of the diffusion constant of the branch point and the corresponding drag caused by the short arm on the reptating long arms. A recent study of 1,4-PI H-polymers also used eq 11 to describe the diffusion of the branch points, and it was found that the theory predicted a smaller terminal time than was measured in this case as well.[10] However, adjusting the value of p^2 to $p^2 = 1/6$ gives a good fit to the rheology data, when combined with corrections for polydispersity (see below).[22] A value of p^2 somewhat less than unity is physically reasonable, as the branch point may not make a full hop every arm retraction time. We thus repeat our calculations and adjust p^2 to fit the data. Since the results of Figure 7 for dynamics in skinny tubes overpredict the terminal time for samples as47 and as37, we no longer consider this case, although we note that we require a value of about $p^2 = 1/30$ to fit the as11 data. Figure 10 shows the results of adjusting p for reptation in dilated tubes with hops in skinny tubes; as47 and as37 are best fit with $p^2 = 1$ as shown before in Figure 8, whereas the other two samples are best fit with $p^2 = 1/7$ and $p^2 = 1/40$ for as17 and as11, respectively. Figure 11 likewise shows the results for reptation and hops in dilated tubes, which were the assumed dynamics in fitting the H-polymers of ref 10. Here we require values of about $p^2 = 1/4$, $1/4$, $1/20$, and $1/60$, for samples as47, as37, as17, and as11, respectively. Thus, the value of p^2 required to fit the data is dependent on the length of the short arm. Also, for the samples with the longest short arms, we cannot get excellent fits simultaneously to both G' and G'' and have settled for a compromise value. Nevertheless, the theory now gives reasonably good fits to the entire series of stars, including the shapes of the spectra as well as the terminal times. The values of p^2 used for the stars with intermediate-length short arms are similar to those needed to fit H-polymers, whereas the small values of p^2 for the stars with short third arms indicate that these arms are causing an anomalously large amount of drag.

The question is thus what is the missing piece of physics that leads to the extra drag caused by the short arms. One possibility is that there is something peculiar about polyisoprene stars. However, comparisons of the

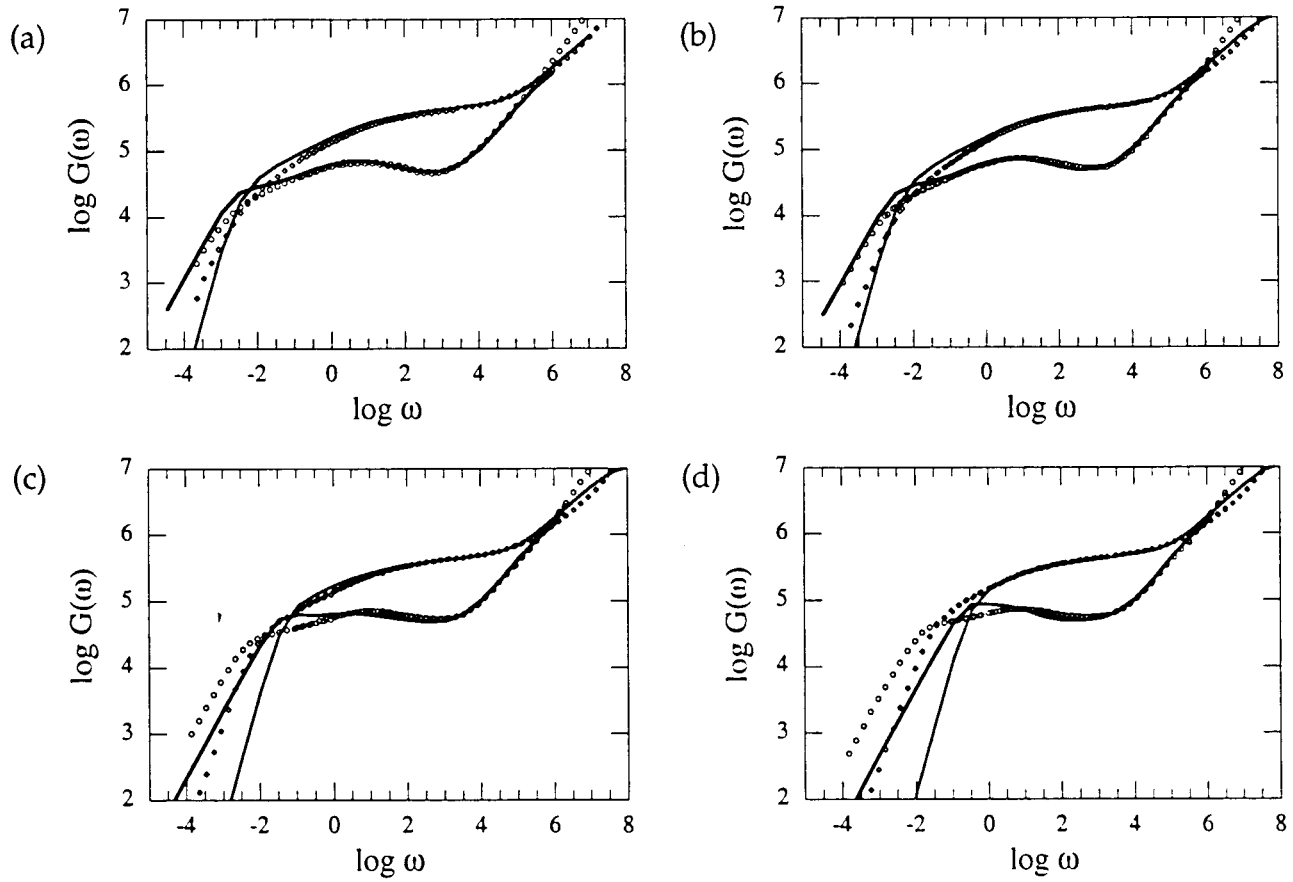

Figure 8. Reptation in dilated tubes, hops in skinny tubes: Data and theoretical predictions of $G'(\omega)$ (diamonds) and $G''(\omega)$ (open circles) for the asymmetric stars with $p^2 = 1$: (a) as47, (b) as37, (c) as17, and (d) as11.

theory with $p = 1$ to the data on PEP stars of Gell et al.[12] display similar discrepancies, although the implementation of the fits is more ambiguous in that case due to uncertainties in the value of τ_e and in the arm molecular weights. Nevertheless, it is clear that the theory predicts a much shorter terminal time than is measured for PEP as well, even for an asymmetric star with a short arm that is slightly less than an entanglement length. Even smaller factors of p^2, in the range of $p^2 = 1/50$ to p^2 on the order of a few hundredths, appear necessary to bring the theory into agreement with the data. Furthermore, the theory and experiment are in good agreement for PI H-polymers with $p^2 = 1/6$,[10] so it is unlikely that chemistry is playing a role in the discrepancy found here.

This large discrepancy between theory and experiment for samples as17 and as11 is most likely not due to errors in the arm molecular weight determinations. For example, to obtain the correct terminal time with $p^2 = 1/6$ for sample as11, with a short arm length of M_s = 11 500 g/mol corresponding to $n_s = M_s/M_e = 2.5$, requires an increase of n_s by a factor of 1.6 to $n_s = 4$, for reptation in a dilated tube and hops in skinny tubes. For hops in dilated tubes, we need $n_s = 4.5$, corresponding to M_s = 20 500 g/mol, to fit the data for as11. It is unlikely that the measured molecular weight is wrong by this amount.

Since it seems for the asymmetric PI stars that theory and experiment only disagree for the stars with quite short third arms, consisting of about 2.5 and 4 entanglement lengths, one may reasonably ask whether the theory is valid for such short arms. In particular, the validity of dynamic dilution depends on a separation of relaxation times along the star arm, which does not hold for sufficiently short arms. However, studies of symmetric star polymers found the theory in excellent agreement with data down to $M/M_e \approx 3$.[6] The theory works well for an H-polymer with arms of length $M/M_e = 5.2$[10] and for a comb polymer with arms of length $M/M_e = 6.3$.[11] Furthermore, we find we need an anomalously small value of p^2 to fit all of the asymmetric PEP stars studied by Gell et al., including one with short arm length $M_s/M_e \approx 9.8$.

One possible source of the discrepancy is polydispersity in the arm lengths. Polydispersity was identified to be important in the rheology of H-shaped polymers,[10] whose relaxation is very similar to that of the asymmetric polymers described here. In the H-polymers, the dangling arms relax by arm retraction with dynamic dilution as described in section 2. The backbone of the H-polymer remains immobile until after the dangling arms have relaxed; the two branch points in the H-polymer can make diffusive hops each time an arm retracts fully to the branch point, analogously to the situation for the asymmetric stars. At long times the backbone relaxes by contour-length fluctuations and finally by reptation, dragging the dangling arms with it. The theory describing the H-polymer relaxation is thus very similar to that for the asymmetric stars, with appropriate modifications for the presence of two branch points.[10] The authors of ref 10 argued that even the small amounts of polydispersity present in anionically synthesized samples is enough to significantly modify the relaxation spectra for H-polymers and found that inclusion of polydispersity effects led to reasonable fits to data on a series of 1,4-PI H-polymers.

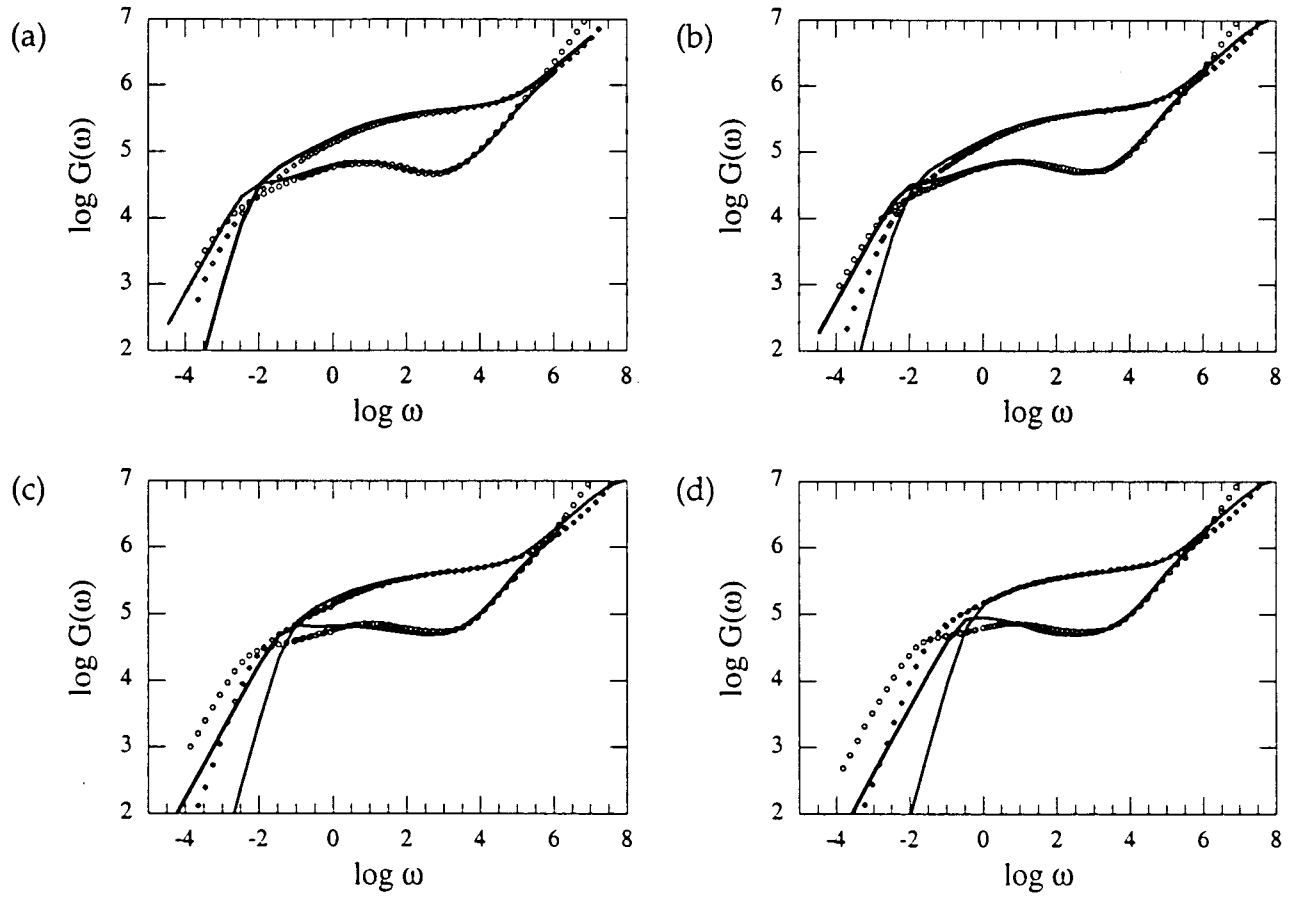

Figure 9. Reptation in dilated tubes, hops in dilated tubes: Data and theoretical predictions of $G'(\omega)$ (diamonds) and $G''(\omega)$ (open circles) for the asymmetric stars with $p^2 = 1$: (a) as47, (b) as37, (c) as17, and (d) as11.

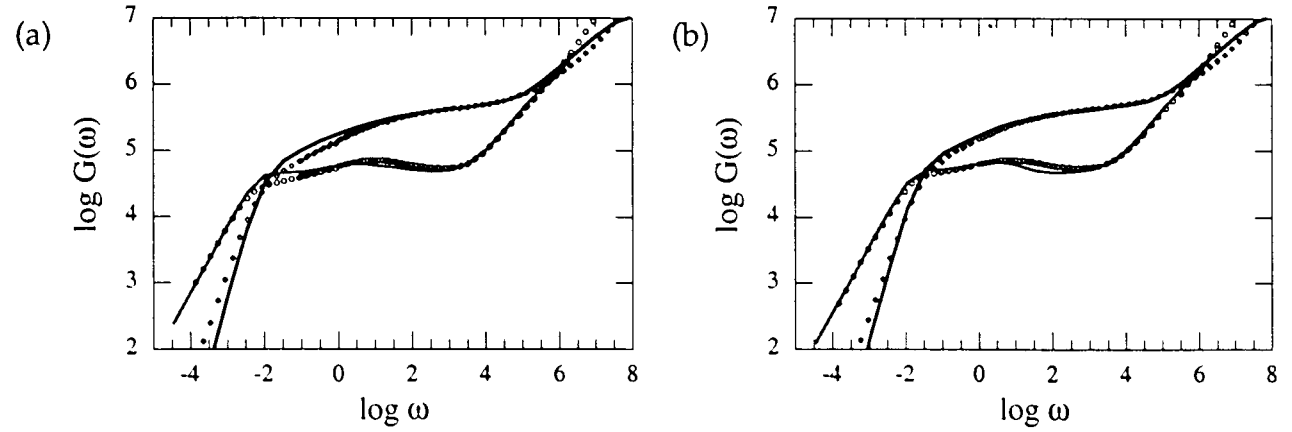

Figure 10. Reptation in dilated tubes, hops in skinny tubes: Data and theoretical predictions of $G'(\omega)$ (diamonds) and $G''(\omega)$ (open circles) for the asymmetric stars with (a) as17, $p^2 = {}^1/_7$ (b) as11, $p^2 = {}^1/_{40}$.

We have reconsidered the treatment of polydispersity effects in both asymmetric stars and H-polymers. The results differ in detail from those of ref 10, so we present them here. We begin by reviewing the effects of polydispersity in more simple situations. First consider dilute, polydisperse, symmetric stars in a fixed network. In this situation, each relaxing star arm is independent of the others and there is no dynamic dilution. The terminal time for each star arm is simply given by the Pearson−Helfand potential for arm retraction in a fixed network, $\tau(s) \sim \exp[U(s)] = \exp[\nu n s^2]$, where $n = M_a/M_e$. The terminal time for the entire system will thus be the relaxation time of the longest arm, $\tau_{max} = \tau(s = 1) \sim \exp(\nu n_{max})$. The situation is quite different in a melt. Ball and McLeish showed that in a polydisperse symmetric star melt, the terminal time is given by the relaxation time of an arm with the weight-averaged molecular weight M_w:[4]

$$\tau_{max} = \tau(s = 1) \propto \exp(\nu \bar{n}/3) \qquad (24)$$

where $\bar{n} = M_w/M_e$. This result, known as motional narrowing, is an effect of dynamic dilution. The presence of the longer arms slows the relaxation of the shorter ones compared to their relaxation time in a monodisperse melt, and the shorter arms speed the relaxation of the longer arms by diluting the network more quickly than a monodisperse melt of long arms would. Thus,

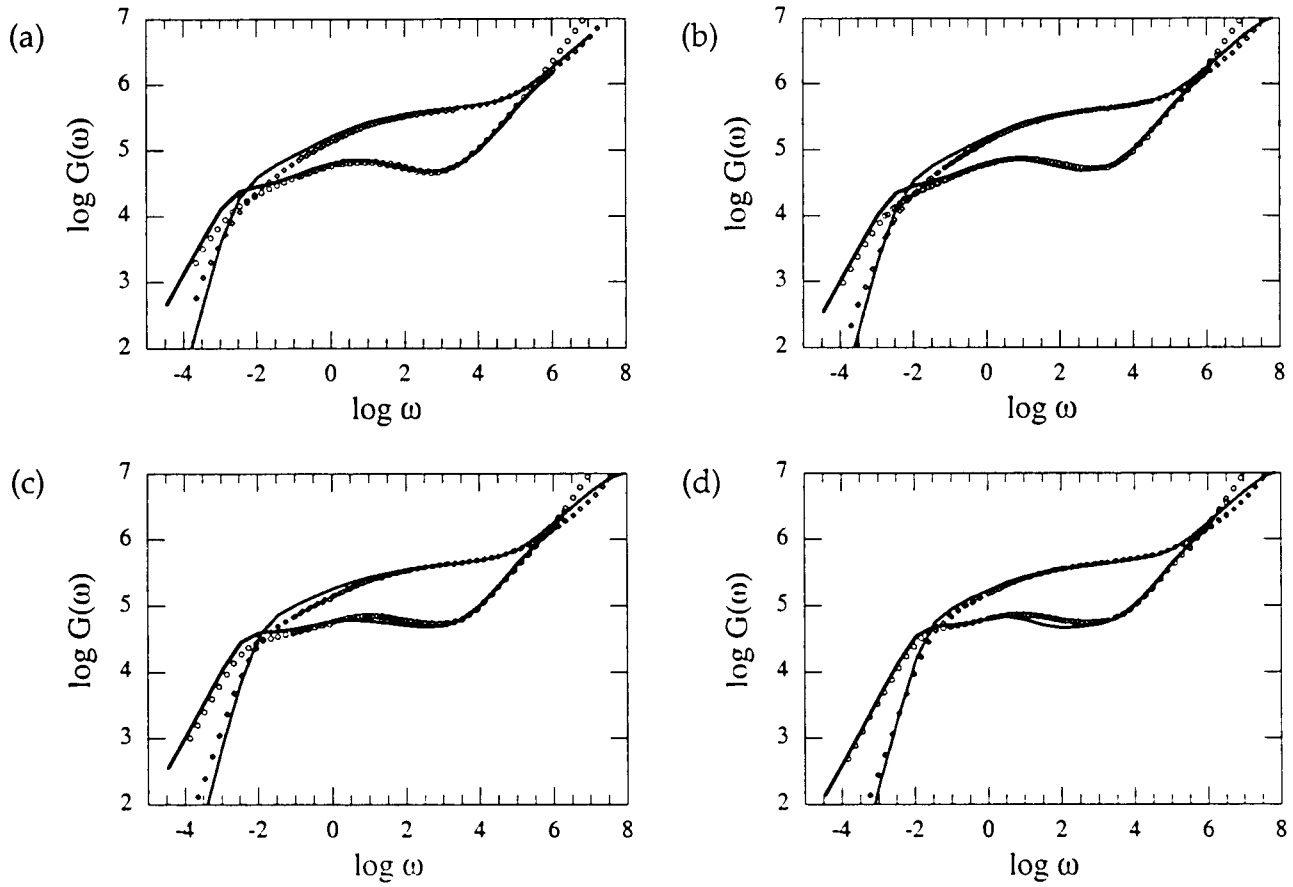

Figure 11. Reptation and hops in dilated tubes: Data and theoretical predictions of $G'(\omega)$ (diamonds) and $G''(\omega)$ (open circles) for the asymmetric stars with (a) as47, $p^2 = 1/4$, (b) as37, $p^2 = 1/4$, (c) as17, $p^2 = 1/20$, and (d) as11, $p^2 = 1/60$.

the spectrum of relaxation times in a polydisperse melt is more narrow than the range of relaxation times of the equivalent monodisperse systems.

In calculating the stress relaxation in asymmetric stars or H-polymers, we would like to know how polydispersity affects the average relaxation time of an arm, since we expect the effective diffusion constant of the branch points to depend on the average arm retraction time. We show in Appendix B that for a unimodal melt of arms, a small amount of polydispersity always *reduces* the average arm relaxation time below the relaxation time of an arm with the mean length (i.e., below the terminal time).

Polydispersity effects are important in H-polymers because the backbone of the H-polymer is immobile during the relaxation of the arms. This reduces the amount of motional narrowing that can occur, since the arm relaxation is occurring in an entanglement network that is partially fixed. In this case polydispersity in the arms leads to a *longer* mean arm relaxation time than the relaxation time of an arm with the mean length, since longer arms take longer to relax in a fixed network. A similar effect could occur in the asymmetric stars, especially when the third arm is short. In this case, the portions of the long arms which have not relaxed by the short arm retraction time τ_s^* also form an immobile volume fraction of the entanglement network.

In Appendix B, we calculate the mean arm relaxation time for a volume fraction ϕ_a of mobile, polydisperse arms, immersed in an immobile volume fraction $\phi_b = 1 - \phi_a$. The calculation uses the Ball−McLeish equation (eq 3) to find the log relaxation time $\ln \tau(n)$ of an arm of length n, with $\alpha = 1$ for simplicity. The number-average of the arm relaxation time is then

$$\langle \tau \rangle = \int_0^\infty \mathrm{d}n \, \frac{\phi(n)}{n} e^{\ln \tau(n)} / \int_0^\infty \mathrm{d}n \, \phi(n)/n \qquad (25)$$

where $\phi(n)$ is the mass distribution of arms. The polydispersity is characterized by $M_w/M_n = 1 + \epsilon$ where ϵ is small for anionically synthesized polymers. Assuming that $\phi(n)$ is Gaussian, $\phi(n) = \exp[-(n - \bar{n})^2/2\Delta^2]/(\sqrt{2\pi}\Delta)$ with $\epsilon = \Delta^2/\bar{n}^2$, we find to leading order in ϵ that

$$\langle \tau \rangle \approx \exp[\nu \phi_a \bar{n}/3] \exp[\nu \phi_b \bar{n} + \nu^2 \phi_b{}^2 \bar{n}^2 \epsilon/2] \qquad (26)$$

The first exponential reflects the motional narrowing due to the dynamic dilution of the arms by themselves, whereas the second exponential reflects the contribution from the fixed part of the network, with volume fraction ϕ_b. We see that small amounts of polydispersity lead to longer average relaxation times for arms in a partially fixed network. Equation 26 is an upper bound on $\langle \tau \rangle$, since some factors of order unity that have been left out, as well as the second-order corrections, decrease the value of $\langle \tau \rangle$ in eq 26.

The first question to ask is how significant the correction to the arm relaxation time is for the samples of interest. From eq 26, small amounts of polydispersity will increase the average arm relaxation time (above the relaxation time of an arm of mean length) by a factor of $\exp[\nu^2 \phi_b{}^2 \bar{n}^2 \epsilon/2]$. For the H-polymers, the immobile volume fraction is simply the backbone volume fraction $\phi_b = n_b/(4n_a + n_b)$, where n_a and n_b are the molecular

Table 2. Increases in Relaxation Times Due to Polydispersity

sample	$\exp[\nu^2\phi_b^2\bar{n}^2\epsilon/2]$
H110B20A	1.2
H160B40A	3.5
H110B52A	1.6
H200B65A	3.6
as47	1.3
as37	1.3
as17	1.4
as11	1.2

weights of the arms and backbone, respectively, in units of M_e. The values of n_a, n_b, and the polydispersity of the arms ϵ_a are tabulated in Table 2 of ref 10 for the four samples studied. Using these values, we find the increases in $\langle\tau\rangle$ shown in Table 2. The increases are significant for all the H-polymers except sample H110B20A.

The immobile volume fraction in the asymmetric star polymers can be estimated as the volume fraction of the long arms which remain unrelaxed at the short arm relaxation time. This is simply $\phi_b = (1 - s_l^*)\phi_l$, where s_l^* is found from equating the long arm relaxation time with the short arm relaxation time, $\tau_{l1}(s_l^*) = \tau_s(s_s = 1) = \tau_s^*$. The polydispersities of the short star arms can be found from Table 1, which tabulates $M_w/M_n = 1 + \epsilon$. The resulting increases in τ_s^* due to polydispersity are also shown in Table 2. We see that the small amounts of polydispersity present have a negligible effect on the short arm relaxation times for all of the asymmetric stars studied. This is because either (1) the short arms are quite short, so that the exponential dependence of τ_s^* on $\bar{n}^2\epsilon$ is weak, or (2) when the short arms are longer, large portions of the long arms relax while the short arms are relaxing, so that the overall immobile volume fraction ϕ_b is small. Thus, polydispersity does not lead to any noticeable increase in the relaxation times of the asymmetric stars, and cannot reduce the large drag (small p^2) which must be assumed to fit the data.

We can, however, calculate the effects of arm polydispersity on the spectra of the H-polymers with a few approximations. We have recalculated the theoretical predictions for $G^*(\omega)$ for the H-polymers studied in ref 10. Since the best-case scenario for the asymmetric stars (i.e., that with the largest values of p^2 required to the fit the data) is the one in which the branch point hops in a "skinny" tube, we calculate the H-polymer moduli assuming that the branch points hop in undilated skinny tubes, rather than in dilated tubes as was assumed in ref 10. Thus, we use eq 11 with $a_h = a$ (divided by two to account for the two arms at each branch point) in place of eq 32 in ref 10. The early time contour-length fluctuations of the backbone and the reptation time are thus both reduced by a factor of ϕ_b^α compared to eqs 34 and 42 of ref 10, due to the branch points hopping in skinny tubes. We also use the full Doi−Edwards spectrum for the reptation of the backbone, rather than a single contribution due to relaxation at τ_d.

The effects of polydispersity in the arms on the spectra are calculated approximately in Appendix B. They can be written as an additive correction $\delta G(t)$ to the loss modulus due to small polydispersity. The full modulus is then taken to be the modulus calculated in ref 10 (with the changes discussed above) plus the correction from eq B52 below, using the correction to the mean arm relaxation time given by eq 26 through-

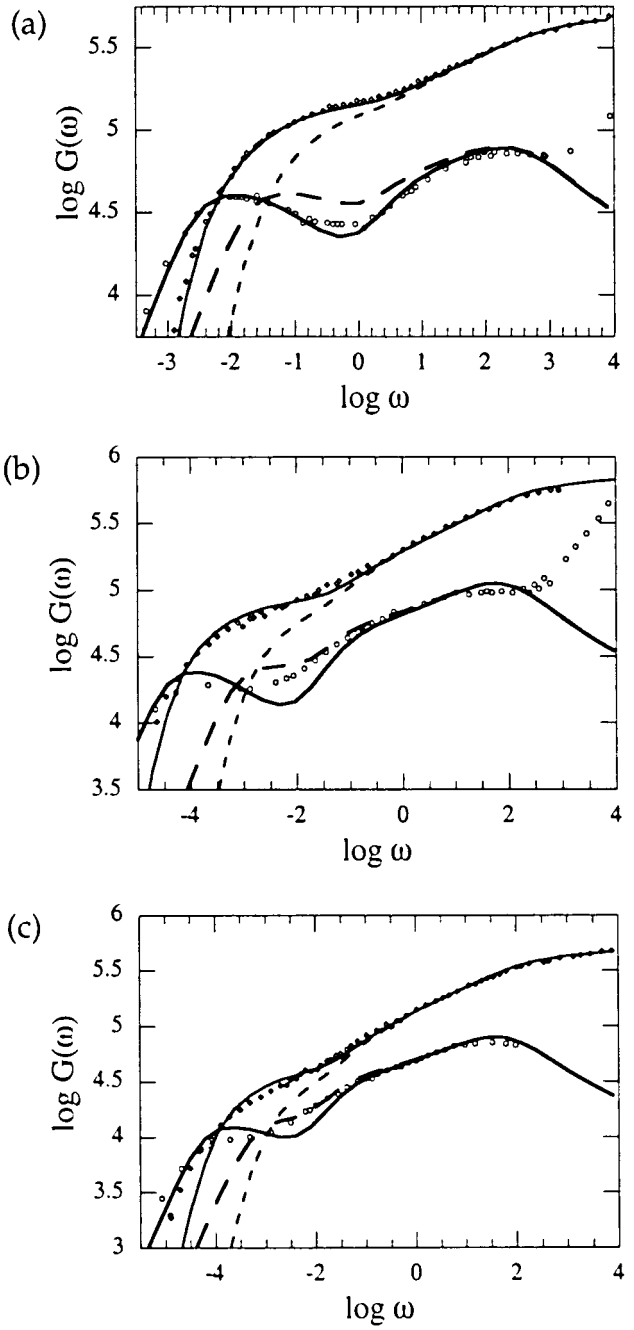

Figure 12. Data from ref 10 and theoretical predictions of $G'(\omega)$ (diamonds) and $G''(\omega)$ (open circles) for three H polymer samples: (a) H110B20A; (b) H160B40A; (c) H110B52A. The dashed curves are the present theory of section 4 with $p = 1$ and no polydispersity corrections, while the solid curves are for $p^2 = 1/6$ with polydispersity corrections as outlined in the text (the polydispersity corrections in part a are negligible).

out. Using the same values of n_a, n_b, G_N^0, and τ_e as ref 10, and using the calculated values of the polydispersity in the arms ϵ_a, we find that we can fit the first three samples with a common value of $p^2 = 1/6$. Figure 12 shows the data from ref 10 along with the predicted moduli for two cases: 1) $p = 1$ and no polydispersity corrections, and 2) $p^2 = 1/6$ with polydispersity corrections. Polydispersity leads to almost no correction for sample H110B20A, so we did not include any polydispersity effects in Figure 12a.

The theory shows similar discrepancies to the case found for the asymmetric stars when $p^2 = 1$ and polydispersity effects are not included. We see that the

theory correctly predicts the terminal times for all three samples when $p^2 = 1/6$ and polydispersity is included. The shape of the spectra for sample H110B20A are also well-fit by the theory, with no polydispersity corrections. The shape of the calculated spectra for the other two samples display more variation than the data, particularly for sample H160B40A which had the largest polydispersity correction. This may be due to the approximations used in calculating $\delta G(t)$. We found that we could also fit the data for samples H160B40A and H110B52A without including any effects of polydispersity, by decreasing the value of p^2 to $1/15$ and $1/12$, respectively. However, for this case the shapes of the spectra remain essentially the same as those shown in Figure 12, parts b and c.

Thus, small amounts of polydispersity in the arms are sufficient to give agreement between theory and data for 1,4-PI H polymers, with a physically reasonable value of the parameter p which is independent of the polymer molecular weight. However, polydispersity has a negligible effect on the spectra of the asymmetric star polymers studied here.

One final possibility for the source of the discrepancy concerns the calculation of the activated arm retraction time. The arm relaxation time given by eq 8 was calculated from the first-passage time of the arm free end to a point s. The calculation in effect only considered the longest Rouse mode of the arm. A recent solution to the first passage time problem for the full range of Rouse modes of a retracting star arm in a fixed network indicates that $\tau_a(s)$ may be too large in eq 8 by a factor of $n = N/N_e$.[23] This may help with the present discrepancy as follows. We fit the value of N_e based on the linear and symmetric star polymers, which have roughly the same molecular weights as the long arms of the asymmetric stars. If our calculated relaxation times $\tau_a(s)$ are actually too long, then we would have used a value of N/N_e that was too small and thus a value of N_e that was somewhat too large. The resulting values for the short arm lengths, $n_s = N_s/N_e$, would be correspondingly too short, leading to the prediction of terminal times that are shorter than measured. This effect would become more pronounced as n_s grew shorter, which would explain the molecular weight dependence of our fitted values for p^2. We note that this effect would be most pronounced in asymmetric stars. Further investigation of the connection between the first passage time and the stress relaxation is thus warranted, especially for short star arms.

5. Conclusions

We have presented data on the linear rheology of a well-defined series of 1,4-PI asymmetric stars, covering the full range of relaxation mechanisms in these systems. The data show a crossover in terminal times from the symmetric star limit toward the linear chain limit as the length of the short arm decreases, although all the star terminal times are significantly longer than that for the linear chain. Furthermore, the shapes of the spectra are more starlike than linear-like for all the asymmetric stars studied.

We have also extended previous successful theories for stress relaxation in symmetric stars and in linear polymers to calculate $G^*(\omega)$ for the asymmetric stars. There is essentially only one unknown parameter in the theory for the asymmetric stars, the fraction p of a tube diameter that the branch point hops each short arm retraction time. All other parameters can be found from the properties of the linear polymer. We find good agreement between theory and experiment for two of the asymmetric stars (those with the longer sidearms most nearly approaching half the molecular weight of the linear molecule), using physically reasonable values of $p^2 = 1$ or $p^2 \approx 1/4$, depending on the assumed dynamics of the branch point hopping. However, we find that for the two samples with the shortest third arms it is necessary to assume very low values of p^2, such that the short arm of the asymmetric stars causes an unusually large amount of drag on the backbone consisting of the two long arms, to bring the theory into agreement with the data. This situation also holds true for comparisons of the theory with the data on asymmetric PEP stars of Gell et al.[12] In that case, one of the stars had a short arm that consisted of less than an entanglement length, yet this was still sufficient to slow the terminal time markedly compared to that of a linear chain with the same "arm" length.

Our result is all the more puzzling because a similar problem does not appear to occur in 1,4-PI H-polymers, which are similar to the asymmetric stars in many respects. An analysis of the possible effects of polydispersity shows that a small amount of polydispersity in the arms does lead to longer terminal times in the H-polymers, but for the molecular weight ranges studied here polydispersity has a negligible effect on the dynamics of the asymmetric star polymers. Thus, the theory is in agreement with the data for the H-polymers, using a physically reasonable value for the amount of drag caused by the dangling arms and including polydispersity effects, but does not fit all of the asymmetric star data.

It seems that there must be some physical mechanism that occurs in three-arm asymmetric stars but not in other polymer systems previously investigated with these types of tube model theories (symmetric stars, H-polymers, star−star blends, star−linear blends, and combs). One possibility is that we need to rethink the calculation of the activated arm retraction times. Another is that we are missing some physics that has to do with the motion of the branch point. We note that it is still unclear whether the branch point should be thought of as hopping in a dilated or in an undilated tube. Further experiments would be helpful in elucidating the apparent discrepancies. The ideal situation would be to use the same batch of long arms to synthesize a series of asymmetric stars with varying short arm lengths, spanning the critical range of about $3N_e - 10N_e$. An understanding of this anomalously slow dynamics of the branch point in asymmetric star melts will be important to furthering our ability to model and understand branched polymer melts.

Acknowledgment. We thank the reviewers for their critiques, which led to much improvement in the paper, and Jung Hun Lee for his comments. Financial support from EPSRC (U.K.) for the synthesis and rheology work is gratefully acknowledged.

Appendix A: Arm Retraction Times

Here we calculate in detail the activated arm retraction times $\tau_{a,i}(s)$, starting from the general Ball−McLeish equation, eq 6:

$$\frac{\mathrm{d}(\ln \tau)}{\mathrm{d}y} = \nu\Phi^{\alpha} \equiv \frac{\mathrm{d}U_{\mathrm{eff}}(y)}{\mathrm{d}y} \tag{A1}$$

We consider the two different time regimes in the activated ($U_{\mathrm{eff}} > k_{\mathrm{B}}T$) arm retraction separately. Thus, we define $\tau_{\mathrm{a,s}}$ to be the retraction time for the short arms, $\tau_{\mathrm{a,l1}}$ to be the retraction time for the long arms before the short arm retraction time τ_{s}^{*}, and $\tau_{\mathrm{a,l2}}$ to be the long arm retraction time after τ_{s}^{*}. Substituting for Φ from eq 7, eq A1 becomes for $y < n_{\mathrm{s}}$, corresponding to $s_{\mathrm{s}} < 1$,

$$\frac{\mathrm{d}(\ln \tau)}{\mathrm{d}y} = \nu\left[\phi_{\mathrm{s}}\left(1 - \sqrt{\frac{y}{n_{\mathrm{s}}}}\right) + \phi_{\mathrm{l}}\left(1 - \sqrt{\frac{y}{n_{\mathrm{l}}}}\right)\right]^{\alpha} = \nu\left[1 - \left(\frac{\phi_{\mathrm{s}}}{\sqrt{n_{\mathrm{s}}}} + \frac{\phi_{\mathrm{l}}}{\sqrt{n_{\mathrm{l}}}}\right)\sqrt{y}\right]^{\alpha} = \frac{\mathrm{d}U_{\mathrm{eff}}}{\mathrm{d}y} \tag{A2}$$

where we have used $\phi_{\mathrm{s}} + \phi_{\mathrm{l}} = 1$. Integrating eq A2 gives the effective potential for $y < n_{\mathrm{s}}$

$$U_{\mathrm{eff}}(y) = 2\nu\frac{1 - (1 - g\sqrt{y})^{\alpha+1}\,[1 + (1+\alpha)g\sqrt{y}]}{g^{2}(1+\alpha)(2+\alpha)} \tag{A3}$$

where

$$g = \frac{\phi_{\mathrm{s}}}{\sqrt{n_{\mathrm{s}}}} + \frac{\phi_{\mathrm{l}}}{\sqrt{n_{\mathrm{l}}}} \tag{A4}$$

and we have set $U_{\mathrm{eff}}(y = 0) = 0$. The effective potential can be rewritten in terms of the fractional distances retracted on each arm, $s_i = \sqrt{y/n_i}$, to give

$$U_{\mathrm{eff,s}}(s_{\mathrm{s}}) = 2\nu n_{\mathrm{s}}\frac{1 - (1 - g_{\mathrm{s}}s_{\mathrm{s}})^{\alpha+1}\,[1 + (1+\alpha)g_{\mathrm{s}}s_{\mathrm{s}}]}{g_{\mathrm{s}}^{2}(1+\alpha)(2+\alpha)} \tag{A5}$$

with $g_s = \phi_{\mathrm{s}} + \phi_{\mathrm{l}}\sqrt{n_{\mathrm{s}}/n_{\mathrm{l}}}$ for the short arm and

$$U_{\mathrm{eff,l1}}(s) = 2\nu n_{\mathrm{l}}\frac{1 - (1 - g_{\mathrm{l}}s_{\mathrm{l}})^{\alpha+1}\,[1 + (1+\alpha)g_{\mathrm{l}}s_{\mathrm{l}}]}{g_{\mathrm{l}}^{2}(1+\alpha)(2+\alpha)} \tag{A6}$$

with $g_{\mathrm{l}} = \phi_{\mathrm{s}}\sqrt{n_{\mathrm{l}}/n_{\mathrm{s}}} + \phi_{\mathrm{l}}$ for the long arms. After the short arm has retracted, $y > n_{\mathrm{s}}$, the Ball−McLeish equation becomes

$$\frac{\mathrm{d}(\ln \tau)}{\mathrm{d}y} = \nu\phi_{\mathrm{l}}^{\alpha}\left(1 - \sqrt{\frac{y}{n_{\mathrm{l}}}}\right)^{\alpha} = \frac{\mathrm{d}U_{\mathrm{l2,eff}}(y)}{\mathrm{d}y} \tag{A7}$$

Integrating eq A7 and changing variables back to s, the effective potential for the long arms after the short arm has retracted is then

$$U_{\mathrm{eff,l2}}(s) = 2\nu n_{\mathrm{l}}\phi_{\mathrm{l}}^{\alpha}\frac{1 - (1 - s)^{\alpha+1}\,[1 + (1+\alpha)s]}{(1+\alpha)(2+\alpha)} + c \tag{A8}$$

The integration constant c is determined by requiring continuity at $y = n_{\mathrm{l}}s_{\mathrm{l}}^{2} = n_{\mathrm{s}}$ in the effective potential for the long arms

$$U_{\mathrm{eff,l1}}(s_{\mathrm{l}} = \sqrt{n_{\mathrm{s}}/n_{\mathrm{l}}}) = U_{\mathrm{eff,l2}}\,(s_{\mathrm{l}} = \sqrt{n_{\mathrm{s}}/n_{\mathrm{l}}}) \tag{A9}$$

As mentioned in section 2, the time $\tau_{\mathrm{a}}(s)$ for an arm to retract a distance s in its effective potential is calculated explicitly in ref 5 by solving a first-passage time problem for the prefactor. We repeat the general result here:

$$\tau_{\mathrm{a}}(s) = (L^{2}/D_{\mathrm{eff}})\int_{0}^{s}\mathrm{d}s'\,\exp[U_{\mathrm{eff}}(s')]\int_{-\infty}^{s'}\mathrm{d}s''\,\exp[-U_{\mathrm{eff}}(s'')] \tag{A10}$$

D_{eff} is the effective curvilinear diffusion constant of the retracting arm. When the effective potential $U_{\mathrm{eff}}(s)$ has a finite slope for all s, the activated retraction time is well approximated by eq 19 from ref 5:[24]

$$\tau_{\mathrm{a}}(s) \approx \frac{L^{2}}{D_{\mathrm{eff}}}\frac{\exp[U_{\mathrm{eff}}(s)]}{U'_{\mathrm{eff}}(s)}\left(\frac{2\pi}{U''_{\mathrm{eff}}(0)}\right)^{1/2} \tag{A11}$$

However, if U'_{eff} becomes sufficiently small, this approximation is no longer accurate. This is the case for asymmetric stars as we approach the symmetric star limit; when the length of the short arm is close to that of the long arms, the derivative of U_{eff} becomes small near $s = 1$ and so $\tau_{\mathrm{a}}(s)$ from the above expression begins to diverge. We thus need a better approximation to eq A10 near $s = 1$. The inner integral is well approximated by $[2\pi/U''_{\mathrm{eff}}(0)]^{1/2}$.[5] First consider the short and long arm effective potentials before the short arm retraction time ($y < n_{\mathrm{s}}$), eqs A5 and A6. We expand $U_{\mathrm{eff,i}}(s)$ in the outer integrand in eq A10 near $s_i = 1$, obtaining

$$U_{\mathrm{eff},i}(s_i) \approx U_{\mathrm{eff}}(1) - \frac{15n_i}{4g_i^{2}}\frac{(1 - g_is_i)^{1+\alpha}}{1+\alpha} \tag{A12}$$

Integrating, we find near $s_i = 1$

$$\tau_{\mathrm{a},i}(s_i) \approx \frac{L^{2}}{D_{\mathrm{eff},i}}\exp[U_{\mathrm{eff},i}(s_i)]\left(\frac{2\pi}{U''_{\mathrm{eff},i}(0)}\right)^{1/2}\frac{(1+\alpha)^{-\alpha/(1+\alpha)}}{g_i}\left(\frac{15n_i}{4g_i^{2}}\right)^{-1/1+\alpha}\Gamma\left(\frac{1}{1+\alpha}\right) \tag{A13}$$

We can combine this result with eq A11 into a crossover function, following ref 5, to obtain an expression for the activated retraction time for all s_i:

$$\tau_{\mathrm{a},i}(s_i) = \tau_{\mathrm{e}}n_i^{3/2}\left(\frac{2\pi^{5}}{15}\right)^{1/2}\frac{\exp[U_{\mathrm{eff},i}(s_i)]}{s_i\left[(1 - g_is_i)^{2\alpha} + \frac{1}{g_i^{2}}\left(\left(\frac{g_i^{2}}{2\nu n_i}\right)(1+\alpha)\right)^{2\alpha/(\alpha+1)}\Gamma\left(\frac{1}{\alpha+1}\right)^{-2}\right]^{1/2}} \tag{A14}$$

where $i =$ s, l1 refers to either the short arms or the long arms before the short arm retraction time.

The effective potential $U_{\mathrm{eff,l2}}$ for the long arms at late times, when $y > n_{\mathrm{s}}$, is simply proportional to that for a symmetric star: $U_{\mathrm{eff,l2}}(s) = \phi_{\mathrm{l}}^{\alpha}U_{\mathrm{eff},star}(s) + c$. The activated arm retraction time in this regime is thus given by eq 28 from ref 5 with appropriate factors of ϕ_{l}:[5,6]

$$\tau_{a,l2}(s_l) = \tau_e \left(\frac{n_l}{\phi_l^{\alpha}}\right)^{3/2} \left(\frac{2\pi^5}{15}\right)^{1/2} \frac{\exp[U_{eff,l2}(s_l)]}{s_l\left[(1-s_l)^{2\alpha} + ([1/(2\nu\phi_l^{\alpha}n_l)][1+\alpha])^{2\alpha/(\alpha+1)}\,\Gamma\left(\frac{1}{\alpha+1}\right)^{-2}\right]^{1/2}} \quad \text{(A15)}$$

The activated retraction time $\tau_{a,s}$ for the short arm and the times $\tau_{a,l1}$ and $\tau_{a,l2}$ for the long arms are combined with the early time result $\tau_{early}(s)$ into crossover functions as given in eq 10 in section 2.

The use of eqs A14 and A15 to calculate the activated arm retraction times with a quantitative calculation of the prefactor has introduced some errors in the correspondence of the retraction times of the short arms with those of the long arms. At the level of the Ball−McLeish equation, all three effective potentials are equal by construction when the short arm has fully retracted at $s_s = 1$:

$$U_{eff,s}(s_s = 1) = U_{eff,l1}\,(s_l = \sqrt{n_s/n_l}) = U_{eff,l2}\,(s_l = \sqrt{n_s/n_l})$$

However, due to the prefactors in the expressions for the $\tau_{a,i}$, the three activated retraction times are not equal at equal values of y, i.e., at $s_s = 1$ and $s_l = \sqrt{n_s/n_l}$:

$$\tau_{a,s}(s_s = 1) \neq \tau_{a,l1}\,(s_l = \sqrt{n_s/n_l}) \neq \tau_{a,l2}\,(s_l = \sqrt{n_s/n_l})$$

The use of the full relaxation times (including the activated and early time fluctuations) τ_s and τ_l as defined by eq 10 exacerbate this problem. We partially adjust for this discrepancy in the calculation of the stress relaxation function $G^*(\omega)$ in eq 17, by changing (in τ_l) from the first expression for the activated relaxation time of the long arms $\tau_{a,l1}$ to the second expression $\tau_{a,l2}$ at a value of $s_l = s_l^*$ found by solving for the distance the long arms have actually retracted at the short arm retraction time:

$$\tau_{l1}(s_l^*) = \tau_s^* = \tau_s(s_s = 1) \quad \text{(A16)}$$

Thus, the full expression for the long arm relaxation time is

$$\tau_l(s) = \begin{cases} t_{l1}(s) = \dfrac{\tau_{early}(s_l)\exp[U_{eff,l1}(s_l)]}{1+\exp[U_{eff,l1}(s_l)]\tau_{early}(s_l)/\tau_{a,l1}(s_l)}, & s_l < s_l^* \\ t_{l2}(s) = \dfrac{\tau_{early}(s_l)\exp[U_{eff,l2}(s_l)]}{1+\exp[U_{eff,l2}(s_l)]\tau_{early}(s_l)/\tau_{a,l2}(s_l)}, & s_l > s_l^* \end{cases} \quad \text{(A17)}$$

We could have chosen instead to switch expressions at $s_l = \sqrt{n_s/n_l}$, where the effective potentials are equal. However, the results for the total retraction time of the long arms, over the entire range of long arm relaxation from $s_l = 0$ to $s_l = s_d$, are nearly identical for these two cases. In either case, the introduced errors are small, since the retraction times are dominated by their exponential dependence on U_{eff}.

Appendix B: Polydispersity Corrections

We are interested in calculating the effect of polydispersity on the relaxation time of some fraction of dangling arms in an entangled polymer melt (asymmetric stars, H-polymers, etc.). For simplicity, we do this at the level of the Ball−McLeish eq 3 for the relaxation times in a diluting network of arms, with $\alpha = 1$. Let s be the fractional distance retracted from the free end of an arm. For monodisperse arms, the relaxation time τ is then simply

$$\frac{d(\ln \tau)}{ds} = 2\nu s \frac{N_a}{N_e(\Phi)} \quad \text{(B1)}$$

where the entanglement length $N_e(\Phi) = N_e/\Phi$, and for a melt of monodisperse arms the entangled volume fraction is $\Phi(s) = 1 - s$. The constant $\nu = {}^{15}/_{8}$. For polydisperse arms, we can change variables in eq B1 to remove the dependence on arm length, to $y = (N_a/N_e)s^2$, so that

$$\frac{d(\ln \tau)}{dy} = \nu\Phi \quad \text{(B2)}$$

1. Melt of Arms. We begin in this first section with a melt of just arms, and later we consider the case in which some fraction of the melt is immobile. In a polydisperse melt of star arms, the unrelaxed volume fraction Φ can be expressed as an integral over the mass distribution $\phi(n)$

$$\Phi(y) = \int_y^{\infty} dn\, \phi(n)(1 - \sqrt{y/n}) \quad \text{(B3)}$$

where $n = N_a/N_e$ and $(1 - \sqrt{y/n})$ gives a factor of $1 - s$ for each arm. Substituting into eq B2 we have

$$\ln \tau(y) = \nu \int_0^y dy'\, \Phi(y') = \nu \int_0^y dy' \int_{y'}^{\infty} dn\, \phi(n)(1 - \sqrt{y'/n}) \quad \text{(B4)}$$

The terminal time for the mixture of polydisperse arms is the longest time, $\tau(\infty)$:

$$\begin{aligned} \ln \tau(\infty) &= \nu \int_0^{\infty} dn \int_0^{n} dy'\, \phi(n)(1 - \sqrt{y'/n}) \\ &= \nu \int_0^{\infty} dn\, \phi(n) n/3 \\ &= \nu \bar{n}/3 \end{aligned} \quad \text{(B5)}$$

where we reversed the order of integration in the first line and $\bar{n}$ is the mass-averaged length of the arms. This result coincides with that of Ball and McLeish.[4]

Next we would like to calculate a mean logarithmic relaxation time for the distribution of arms:

$$\langle \ln\tau \rangle = \int_0^{\infty} dn\, \phi(n) \ln \tau(n) \quad \text{(B6)}$$

where $\tau(n) = \tau(y = n)$ is the relaxation time of an arm of length n (the time for the arm to retract fully to $s = 1$). We rewrite eq B4 and reverse the order of integration:

$$\begin{aligned} \ln \tau(n) &= \nu \int_0^{n} dy \int_y^{\infty} dn' \phi(n')(1 - \sqrt{y'/n}) \\ &= \nu \int_0^{n} dn' \int_0^{n'} dy \phi(n')(1 - \sqrt{y'/n}) + \\ &\quad \nu \int_n^{\infty} dn' \int_0^{n} dy\, \phi(n')(1 - \sqrt{y'/n}) \end{aligned} \quad \text{(B7)}$$

Performing the integral over y gives

$$\ln \tau(n) = \nu \int_0^n \mathrm{d}n'\, \phi(n')n'/3 + \nu \int_n^\infty \mathrm{d}n'\, \phi(n')\left(n - \frac{2\,n^{3/2}}{3_{n'^{1/2}}}\right) \quad \text{(B8)}$$

Adding and subtracting $\int_n^\infty \mathrm{d}n'\, \phi(n')n'/3$ gives

$$\ln \tau(n) = \nu\bar{n}/3 + \nu \int_n^\infty \mathrm{d}n'\phi(n')\left(n - n'/3 - \frac{2\,n^{3/2}}{3_{n'^{1/2}}}\right) \quad \text{(B9)}$$

Averaging over the mass distribution gives the average log time

$$\langle \ln \tau\rangle = \nu\bar{n}/3 + \nu \int_0^\infty \mathrm{d}n\phi(n) \int_n^\infty \mathrm{d}n'\phi(n') \left(n - n'/3 - \frac{2\,n^{3/2}}{3_{n'^{1/2}}}\right) \quad \text{(B10)}$$

Now suppose that $\phi(n)$ is narrowly distributed about its mean $\bar{n}$, so it makes sense to expand n and n' about $\bar{n}$: $n = \bar{n} + \delta n$, $n' = \bar{n} + \delta n'$. Expanding the expression in parentheses above and keeping terms to second order in δn and $\delta n'$, we have

$$\left(n - n'/3 - \frac{2\,n^{3/2}}{3_{n'^{1/2}}}\right) \approx -\frac{1}{4\bar{n}}(\delta n - \delta n')^2 = -\frac{1}{4\bar{n}}(n - n')^2 \quad \text{(B11)}$$

So now the average time is

$$\langle \ln \tau\rangle \approx \nu\bar{n}/3 - \frac{\nu}{4\bar{n}} \int_0^\infty \mathrm{d}n \int_n^\infty \mathrm{d}n'\phi(n)\phi(n')(n - n')^2 \quad \text{(B12)}$$

The integral is now symmetric, so it can easily be evaluated:

$$\begin{aligned}\langle \ln \tau\rangle &\approx \nu\bar{n}/3 - \frac{\nu}{8\bar{n}}\langle n^2 - 2nn' + n'^2\rangle \\ &= \nu\bar{n}/3 - \frac{\nu}{4\bar{n}}\langle (n - \langle n\rangle)^2\rangle \\ &= \frac{\nu\bar{n}}{3}\left(1 - \frac{3\Delta^2}{4\bar{n}^2}\right) \end{aligned} \quad \text{(B13)}$$

where Δ^2 is the variance in n. We would have anticipated the minus sign above, because any average of $\ln \tau(n)$ must be less than the log terminal time $\ln \tau(\infty)$. Furthermore, if the distribution is narrow so that the expansion can be done, we can approximate $\phi(n)$ with a Gaussian, in which case we would expect the first correction to $\ln \tau(\bar{n})$ to be of order Δ^2.

So far we have calculated the average log relaxation time. We may instead be interested in the number average of the relaxation time itself, or

$$\langle \tau\rangle = \int_0^\infty \mathrm{d}n\, \frac{\phi(n)}{n} \mathrm{e}^{\ln\tau(n)} / \int_0^\infty \mathrm{d}n\, \phi(n)/n \quad \text{(B14)}$$

The numerator is

$$\mathrm{Num} = \int_0^\infty \mathrm{d}n\, \frac{\phi(n)}{n} \exp\left[\nu\bar{n}/3 + \nu \int_n^\infty \mathrm{d}n'\phi(n')\left(n - n'/3 - \frac{2\,n^{3/2}}{3_{n'^{1/2}}}\right)\right] \quad \text{(B15)}$$

If $\phi(n)$ is narrow, we can again expand n and n' about $\bar{n}$, so we have

$$\mathrm{Num} \approx \int_0^\infty \mathrm{d}n\, \frac{\phi(n)}{n} \exp\left[\nu\bar{n}/3 - \frac{\nu}{4\bar{n}} \int_n^\infty \mathrm{d}n'\, \phi(n')(n - n')^2\right] \quad \text{(B16)}$$

Also, if $\phi(n)$ is narrow, $(n - n')^2$ is small (of order Δ^2), so we can expand the second exponential:

$$\mathrm{Num} \approx \int_0^\infty \mathrm{d}n\, \frac{\phi(n)}{n} \mathrm{e}^{\nu\bar{n}/3}\left(1 - \frac{\nu}{4\bar{n}} \int_n^\infty \mathrm{d}n'\, \phi(n')(n - n')^2\right) \quad \text{(B17)}$$

Since $(n - n')^2$ is already of $O(\Delta^2)$, we can replace $\phi(n)/n$ with $\phi(n)/\bar{n}$ in the second term, which leads to

$$\langle \tau\rangle \approx \mathrm{e}^{\nu\bar{n}/3}\left(1 - \frac{\nu\Delta^2}{4\bar{n}}\right) \quad \text{(B18)}$$

This is simply $\exp(\langle \ln \tau\rangle)$ from eq B13, to first order in Δ^2.

We have expressed polydispersity corrections in terms of the variance Δ^2 in the mass distribution of arms $\phi(n)$, where the arm length $n = N_\mathrm{a}/N_\mathrm{e} = M_\mathrm{a}/M_\mathrm{e}$. Polydispersity is more commonly described in terms of the difference between the mass- and number-averaged molecular weights: $M_\mathrm{w}/M_n = 1 + \epsilon$ where ϵ is small for anionic polymerizations. In our notation,

$$\frac{M_\mathrm{w}}{M_\mathrm{n}} = \frac{\int \mathrm{d}n\, n\phi(n)}{\int \mathrm{d}n\, \phi(n) / \int \mathrm{d}n\, \frac{\phi(n)}{n}} = \bar{n}\frac{1}{\bar{n}}\left(1 + \frac{\Delta^2}{\bar{n}^2}\right) \quad \text{(B19)}$$

so we can identify $\epsilon = \Delta^2/\bar{n}^2$, where $\bar{n} = M_\mathrm{w}/M_\mathrm{e}$ is the mass averaged molecular weight in units of M_e. In terms of ϵ, eq B18 is

$$\langle \tau\rangle \approx \mathrm{e}^{\nu\bar{n}/3}\left(1 - \frac{\nu\bar{n}\epsilon}{4}\right) \quad \text{(B20)}$$

which gives corrections to first order in $\bar{n}\epsilon$.

For anionic polymerizations, although ϵ is small it may be that $\bar{n}\epsilon = \Delta^2/\bar{n}$ is not small, so that the expansion of the exponential in eq B17 is not valid. We can instead evaluate the full integral in eq B16 using the method of steepest descents. Assuming now that $\phi(n)$ is Gaussian, $\phi(n) = \exp[-(n - \bar{n})^2/2\Delta^2]/(\sqrt{2\pi}\Delta)$, we rewrite eq B16 as

$$\begin{aligned}\mathrm{Num} &\approx \mathrm{e}^{\nu\bar{n}/3} \int_0^\infty \mathrm{d}n \exp\left[-\frac{(n - \bar{n})^2}{2\Delta^2} - \ln \sqrt{2\pi}\Delta - \ln n - \frac{\nu}{4\bar{n}} \int_n^\infty \mathrm{d}n'\phi(n')(n - n')^2\right] \\ &\equiv \mathrm{e}^{\nu\bar{n}/3} \int_0^\infty \mathrm{d}n \exp[f(n)] \end{aligned} \quad \text{(B21)}$$

We can find the location of the peak in the integrand

by differentiating $f(n)$ with respect to n. The peak at n^* satisfies

$$0 = -\frac{n^* - \bar{n}}{\Delta^2} - \frac{1}{n^*} - \frac{\nu}{2\bar{n}}\int_{n^*}^{\infty} dn'\,\phi(n')(n^* - n') \quad \text{(B22)}$$

The peak will be close to $\bar{n}$, so we expand $n^* = \bar{n} + \delta n^*$ and keep the lowest order terms in δn^*:

$$0 \approx -\frac{\delta n^*}{\Delta^2} - \frac{1}{\bar{n}}\left(1 - \frac{\delta n^*}{\bar{n}}\right) - \frac{\nu}{2\bar{n}}\int_{\bar{n}+\delta n^*}^{\infty} dn'\,\phi(n')(n^* - n') \quad \text{(B23)}$$

The integral can be evaluated since we have specified the form of $\phi(n)$:

$$-\frac{\nu}{2\bar{n}}\int_{\bar{n}+\delta n^*}^{\infty} dn'\phi(n')(n^* - n') = -\frac{\nu}{2\bar{n}}\left(\frac{1}{2}\delta n^* - \frac{\Delta}{\sqrt{2\pi}}\exp[-\delta n^{*2}/2\Delta^2] + \frac{\Delta}{\sqrt{2\pi}}\exp[-\bar{n}^2/2\Delta^2] - \frac{1}{2}\delta n^*\,\mathrm{erf}\left(\frac{\delta n^*}{\sqrt{2}\Delta}\right)\right) \approx -\frac{\nu}{2\bar{n}}\left(\frac{1}{2}\delta n^* - \frac{\Delta}{\sqrt{2\pi}}\right) \quad \text{(B24)}$$

In the error function, we have assumed that $\delta n^*/(\sqrt{2}\Delta)$ is small and have neglected terms of this order. From eq B23, we now have to lowest order

$$0 \approx -\frac{\delta n^*}{\Delta^2} - \frac{\nu \delta n^*}{4\bar{n}} + \frac{\nu\Delta}{2\sqrt{2\pi}\bar{n}} \quad \text{(B25)}$$

so that

$$\delta n^* \approx \frac{\nu\Delta^3}{2\sqrt{2\pi}\bar{n}}\left(\frac{1}{1 + \nu\Delta^2/4\bar{n}}\right) \quad \text{(B26)}$$

We see that $\delta n^*/(\sqrt{2}\Delta)$ is reasonably small, even for $\Delta^2 = \bar{n}$ ($\epsilon = 1/\bar{n} = M_e/M_w$), so that the approximations made are valid. Evaluating eq B21 in the same limit of small $\delta n^*/(\sqrt{2}\Delta)$, we find

$$\mathrm{Num} \approx e^{\nu\bar{n}/3}e^{f(n^*)}\frac{\sqrt{2\pi}}{\sqrt{f''(n^*)}} \approx e^{\nu\bar{n}/3}\left(\frac{1}{\sqrt{2\pi}\Delta}\right)\frac{1}{\bar{n} + (\nu\Delta^3/((2\sqrt{2\pi}\bar{n})(1 + \nu\Delta^2/4\bar{n})))} \times \exp\left[-\frac{\nu\Delta^2}{8\bar{n}} - \frac{\nu^2\Delta^4}{(8\pi\bar{n}^2)(1 + \nu\Delta^2/4\bar{n})}\right] \times \frac{\sqrt{2\pi}}{\sqrt{1/\Delta^2 + \nu/4\bar{n} - \nu^2\Delta^2/((8\pi\bar{n}^2)(1 + \nu\Delta^2/4\bar{n}))}}. \quad \text{(B27)}$$

The denominator from eq B14 is of order $1/\bar{n}$, so after some rearrangement, we have

$$\langle\tau\rangle \approx e^{\nu\bar{n}/3}\exp\left[\frac{-\nu\Delta^2}{8\bar{n}}\left(1 + \frac{\nu\Delta^2}{\pi\bar{n}(1 + \nu\Delta^2/4\bar{n})}\right)\right] \times \left(1 + \frac{\nu\Delta^2}{4\bar{n}} - \frac{\nu^2\Delta^4}{(8\pi\bar{n}^2)(1 + \nu\Delta^2/4\bar{n})}\right)^{-1/2} \times \left(1 - \frac{\nu\Delta^3}{2\sqrt{2\pi}\bar{n}^2(1 + \nu\Delta^2/4\bar{n})}\right) \quad \text{(B28)}$$

This result reduces to eq B18 in the limit that $\Delta^2/\bar{n}$ is small. The effect of a small amount of polydispersity in a melt of arms in both cases ($\Delta^2 \ll \bar{n}$ and $\Delta^2 \sim \bar{n}$) is therefore to reduce the average arm relaxation time below the relaxation time for the mean arm length.

2. Melt of Arms with an Immobile Volume Fraction. We now consider the case relevant to melts of H polymers, combs, etc., in which we have some fraction ϕ_a of polydisperse arms and an immobile volume fraction $\phi_b = 1 - \phi_a$. The unrelaxed volume fraction of chains is now

$$\Phi(y) = \phi_a\int_y^{\infty} dn\phi(n)(1 - \sqrt{y/n}) + \phi_b \quad \text{(B29)}$$

so that eq B4 becomes

$$\ln\tau(y) = \nu\int_0^y dy'\,\Phi(y') = \nu\phi_a\int_0^y dy'\int_{y'}^{\infty} dn\,\phi(n)(1 - \sqrt{y'/n}) + \nu\phi_b\int_0^y dy' \quad \text{(B30)}$$

The longest log relaxation time for the arms is now

$$\ln\tau_{max}(y_{max}) = \nu\phi_a\bar{n}/3 + \nu\phi_b y_{max} = \nu\phi_a\bar{n}/3 + \nu\phi_b n_{max} \quad \text{(B31)}$$

where n_{max} is the longest arm in the melt. The first term corresponds to effects of dynamic dilution among the arms, whereas the second term gives the effect of arm relaxation in the fixed part of the network (note that the log terminal time for a single arm in a fixed network is simply $\ln\tau_{max} = \nu n_{max}$). The only difference between eq B30 and eq B4 is the last term, $\nu\phi_b y$, so the average log arm relaxation time is now

$$\langle\ln\tau\rangle \approx \frac{\nu\phi_a\bar{n}}{3}\left(1 - \frac{3\Delta^2}{4\bar{n}^2}\right) + \nu\phi_b\bar{n} \quad \text{(B32)}$$

If we set the immobile volume fraction to zero, $\phi_b = 0$, we recover the previous result of eq B13; if we take $\phi_b = 1$ we obtain the result for dilute arms in a fixed network, in which there is no dynamic dilution so that all the arms relax independently and the average log time is the same as the relaxation time of an arm with the mean length.

The changes due to the immobile volume fraction in the number-average of the relaxation time, $\langle\tau\rangle$ in eq B14, are nontrivial. As before, we first consider the case in which the variance Δ^2 of the arm distribution $\phi(n)$ is quite small, $\Delta^2 \ll \bar{n}$ ($\bar{n}\epsilon \ll 1$). Including the immobile volume fraction, eq B15 becomes

$$\mathrm{Num} = \int_0^{\infty} dn\frac{\phi(n)}{n}\exp\left[\nu\phi_a\bar{n}/3 + \nu\phi_b n + \nu\phi_a\int_n^{\infty} dn'\phi(n')\left(n - n'/3 - \frac{2}{3}\frac{n^{3/2}}{n'^{1/2}}\right)\right] \quad \text{(B33)}$$

We follow the previous development for the melt of

arms. Expanding $n = \bar{n} + \delta n$ as before and keeping lowest order terms in δn, we find

$$\mathrm{Num} \approx \int_0^\infty \mathrm{d}n \frac{\phi(n)}{n} \exp\left[\nu\phi_a\bar{n}/3 + \nu\phi_b(\bar{n} + \delta n) - \frac{\nu\phi_a}{4\bar{n}} \int_n^\infty \mathrm{d}n'\phi(n')(n - n')^2\right]$$

$$\approx \mathrm{e}^{\nu\phi_a\bar{n}/3}\mathrm{e}^{\nu\phi_b\bar{n}} \int_0^\infty \mathrm{d}n \frac{\phi(n)}{n} (1 + \nu\phi_b\delta n + \nu^2{\phi_b}^2\delta n^2/2)\left(1 - \frac{\nu\phi_a}{4\bar{n}} \int_n^\infty \mathrm{d}n'\phi(n')(n - n')^2\right) \quad \text{(B34)}$$

where we have expanded the exponentials in the second line. The lowest order terms then give (note by definition $\langle\delta n\rangle = 0$)

$$\langle\tau\rangle \approx e^{\nu\phi_a\bar{n}/3 + \nu\phi_b\bar{n}}\left(1 - \frac{\nu\phi_a\Delta^2}{4\bar{n}} + \frac{1}{2}\nu^2{\phi_b}^2\Delta^2\right) \quad \text{(B35)}$$

This result reduces to eq B18 in the limit $\phi_b \to 0$. The effect of the immobile volume fraction is to give a polydispersity correction which increases the arm relaxation time; the motional narrowing due to dynamic dilution only occurs for the arm fraction of the melt.

This result is only valid for $\Delta \ll 1$, so we again consider the case in which $\Delta^2/\bar{n}$ (i.e., $\bar{n}\epsilon$) is not small. We again assume that $\phi(n)$ is Gaussian; eq B21 is now

$$\mathrm{Num} \approx e^{\nu\phi_a\bar{n}/3} \int_0^\infty \mathrm{d}n \exp\left[-\frac{(n - \bar{n})^2}{2\Delta^2} - \ln\sqrt{2\pi}\Delta - \ln n + \nu\phi_b n - \frac{\nu\phi_a}{4\bar{n}} \int_n^\infty \mathrm{d}n'\phi(n')(n - n')^2\right] \quad \text{(B36)}$$

The $\nu\phi_b n$ term can be accommodated by shifting the location of the peak in the Gaussian, giving

$$\mathrm{Num} \approx e^{\nu\phi_a\bar{n}/3}e^{\nu\phi_b\bar{n}+\nu^2\phi_b{}^2\Delta^2/2} \int_0^\infty \mathrm{d}n \exp\left[-\frac{(\mathrm{n} - \bar{n}')^2}{2\Delta^2} - \ln\sqrt{2\pi}\Delta - \ln n - \frac{\nu\phi_a}{4\bar{n}} \int_n^\infty \mathrm{d}n'\phi(n')(n - n')^2\right]$$

$$\equiv e^{\nu\phi_a\bar{n}/3}e^{\nu\phi_b\bar{n}+\nu2\phi_b{}^2\Delta^2/2} \int_0^\infty \mathrm{d}n \exp[f(n)] \quad \text{(B37)}$$

where $\bar{n}' = \bar{n} + \nu\phi_b\Delta^2$. Differentiating $f(n)$, the peak position n^* is determined from

$$0 = -\frac{n^* - \bar{n}'}{\Delta^2} - \frac{1}{n^*} - \frac{\nu\phi_a}{2\bar{n}} \int_{n^*}^\infty \mathrm{d}n'\phi(n')(n^* - n') \quad \text{(B38)}$$

We expand $n^* = \bar{n}' + \delta n^*$:

$$0 \approx -\frac{\delta n^*}{\Delta^2} - \frac{1}{\bar{n}'}\left(1 - \frac{\delta n^*}{\bar{n}'}\right) - \frac{\nu\phi_a}{2\bar{n}} \int_{n^*}^\infty \mathrm{d}n'\phi(n')(\bar{n}' - n') \quad \text{(B39)}$$

The lower bound on the integral, $n^* = \bar{n} + \nu\phi_b\Delta^2 + \delta n^*$, is significantly larger than $\bar{n}$ for $\Delta^2 \sim O(\bar{n})$ as long as ϕ_b is not too small. Since $\phi(n')$ is still peaked around $\bar{n}$, we expect the integral itself to be small in this limit. Substituting the Gaussian form for $\phi(n')$ we can simply evaluate the integral:

$$\frac{1}{\sqrt{2\pi}\Delta} \int_{\bar{n}+\nu\phi_b\Delta^2+\delta n^*}^\infty \mathrm{d}n'\mathrm{e}^{-(\mathrm{n}'-\bar{n})^2/2\Delta^2} (\bar{n} + \nu\phi_b\Delta^2 + \delta n^* - n') = -\frac{\Delta}{\sqrt{2\pi}}\mathrm{e}^{-\nu\phi_b/2-\delta n^{*2}/2\Delta^2} + \frac{\nu\phi_b\Delta^2 + \delta n^*}{2} - \frac{1}{2}[\nu\phi_b\Delta^2 + \delta n^*]\,\mathrm{erf}\,(\nu\phi_b\Delta/\sqrt{2} + \delta n^*/\sqrt{2}\Delta)$$

$$\approx -\frac{\Delta}{\sqrt{2\pi}}\mathrm{e}^{-\nu\phi_b/2} \quad \text{(B40)}$$

where we have neglected small terms of order $\delta n^*/\sqrt{2}\Delta$ as before, and we have taken $\mathrm{erf}(\nu\phi_b\Delta/\sqrt{2}) \to 1$ for large $\nu\phi_b\Delta/\sqrt{2}$ in the last line. Note that by using this approximation, we will no longer be able to take the $\phi_b \to 0$ or Δ small limits in the results. From eq B39, to lowest order δn^* is

$$\delta n^* \approx \frac{\nu\phi_a\Delta^3}{2\sqrt{2\pi}\bar{n}}\mathrm{e}^{-\nu\phi_b/2} \quad \text{(B41)}$$

To evaluate eq B37 we need $f(n^*)$ where $n^* = \bar{n} + \nu\phi_b\Delta^2 + \delta n^*$:

$$f(n^*) \approx -\ln\sqrt{2\pi}\Delta - \ln\left(\bar{n} + \nu\phi_b\Delta^2 + \frac{\nu\phi_a\Delta^3}{2\sqrt{2\pi}\bar{n}}\mathrm{e}^{-\nu\phi_b/2}\right) - \frac{\nu\phi_a}{4\bar{n}} \int_{\bar{n}'}^\infty \mathrm{d}n'\phi(n')(n - n')^2 - \frac{\nu^2{\phi_a}^2\Delta^4}{16\pi\bar{n}^2}\mathrm{e}^{-\nu\phi_b/2} \quad \text{(B42)}$$

For large $\nu\phi_b\Delta$, the integral is of order $(\Delta^3/\bar{n})\exp(-\nu^2{\phi_b}^2\Delta^2/2)$, which is small so we neglect it. In the same limit, $f''(n^*) \approx -1/\Delta^2$. Thus, eq B37 is

$$\mathrm{Num} \approx e^{\nu\phi_a\bar{n}/3}e^{\nu\phi_b\bar{n}+\nu^2\phi_b{}^2\Delta^2/2} \frac{1}{\sqrt{2\pi}\Delta\bar{n}(1 + \nu\phi_b\Delta^2/\bar{n})}\left(1 - \frac{\nu\phi_a\Delta^3\mathrm{e}^{-\nu\phi_b/2}}{2\sqrt{2\pi}\bar{n}^2(1 + \nu\phi_b\Delta^2/\bar{n})}\right)\exp\left[-\frac{\nu^2{\phi_a}^2\Delta^4}{16\pi\bar{n}^2}\mathrm{e}^{-\nu\phi_b/2}\right]\sqrt{2\pi}\Delta \quad \text{(B43)}$$

Again the denominator from eq B14 to lowest order is simply $1/\bar{n}$, so the average arm relaxation time is

$$\langle\tau\rangle \approx e^{\nu\phi_a\bar{n}/3}e^{\nu\phi_b\bar{n}+\nu^2\phi_b{}^2\Delta^2/2} \frac{\exp\left[-\frac{\nu^2\phi_a^2\Delta^4}{16\pi\bar{n}^2}e^{-\nu\phi_b/2}\right]}{1 + \nu\phi_b\Delta^2/\bar{n}} \times \left(1 - O\left(\frac{\phi_a\Delta^3}{\bar{n}^2}\right)\right) \quad \text{(B44)}$$

Thus, we find polydispersity leads to two main corrections to the relaxation time of the mean arm length: it decreases the average time by a term which is small and proportional to the fraction of arms ϕ_a, but it increases the average time by a larger amount which depends on the immobile volume fraction ϕ_b. Because of the approximations used in deriving eq B44 we cannot take the $\phi_b \to 0$ limit, but comparing with eq B28 we see the corrections are of the same order, the only differences being in the terms of order unity. Neglecting the factors of order unity, we can rewrite the leading order term in eq B44 in terms of ϵ:

$$\langle\tau\rangle \approx \exp[\nu\phi_a\bar{n}/3]\exp[\nu\phi_b\bar{n} + \nu^2\phi_b{}^2\bar{n}^2\epsilon/2] \quad \text{(B45)}$$

For polydispersities typical of anionic polymerizations, this can lead to significantly longer relaxation times for melts with reasonably large immobile volume fractions and long arms.

3. Effects of Polydispersity on *G*(*t*). We can include the effects of polydispersity in the arms on $G(t)$ for H-polymers as follows. As shown above, the polydispersity effects associated with the dynamically diluting part of the network are small, so we neglect them and focus on the increase in relaxation time due to the immobile volume fraction. This will give us an upper bound on the size of the effects. For this situation, because polydispersity has no effect on the Pearson−Helfand potential for retraction in a fixed network, we know from the Ball−McLeish equation that the function $\ln \tau(y)$ is still given by

$$\ln \tau(y) = \nu\phi_a\left(y - \frac{2}{3}\frac{y^{3/2}}{n^{1/2}}\right) + \nu\phi_b y \quad \text{(B46)}$$

for all $y = ns^2$ (polydispersity only affects the dynamically diluted part of the potential, U_{eff}, which we are ignoring here). We calculate the relaxation modulus from

$$G(t) = -\int_0^\infty dy \frac{\partial G}{\partial \Phi}\frac{\partial \Phi}{\partial y} e^{-t/\tau(y)} \quad \text{(B47)}$$

where $\Phi(y)$ is given in eq B29:

$$\Phi(y) = \phi_a \int_y^\infty dn\phi(n)(1 - \sqrt{y/n}) + \phi_b \quad \text{(B48)}$$

The first factor in the integrand in $G(t)$ describes the effects of dynamic dilution, so we will make no polydispersity corrections in this term. The function $\tau(y)$ is given by eq B46. Thus, the polydispersity corrections only enter into the second factor in the integrand, which describes how much material is left unrelaxed at y. We thus use the weight-averaged molecular weight in the first factor, $n = \bar{n}$, but keep the distribution in the second factor in G:

$$\frac{G(t)}{G_N^0(1+\alpha)} = \int_0^\infty dy \left[\phi_a\left(1 - \sqrt{\frac{y}{\bar{n}}}\right)\theta(y-\bar{n}) + \phi_b\right]^\alpha \phi_a \int_y^\infty dn\,\phi(n)\frac{1}{\sqrt{yn}} e^{-t/\tau(y)} \quad \text{(B49)}$$

where $\theta(y - \bar{n})$ is a step function, ensuring that there are only contributions for $y \le \bar{n}$ in the first factor. For narrow $\phi(n)$ the inner integral is approximately

$$\int_y^\infty dn\phi(n)\frac{1}{\sqrt{yn}} \approx \frac{1}{\sqrt{y\bar{n}}}\int_y^\infty dn\phi(n) \quad \text{(B50)}$$

For a monodisperse system $\phi(n) = \delta(n - \bar{n})$, and the integral above is simply a step function. Thus, we can calculate the correction to $G(t)$ due to having some width to $\phi(n)$ as

$$\frac{\delta G(t)}{G_N^0(1+\alpha)} = \int_0^\infty dy \frac{\phi_a}{\sqrt{y\bar{n}}}\left[\phi_a\left(1 - \sqrt{\frac{y}{\bar{n}}}\right)\theta(y-\bar{n}) + \phi_b\right]^\alpha \times \left[\int_y^\infty dn\,\phi(n) - \theta(y-\bar{n})\right] e^{-t/\tau(y)} \quad \text{(B51)}$$

If we assume $\phi(n)$ to be Gaussian as before, we can evaluate the inner integral explicitly to obtain

$$\frac{\delta G(t)}{G_N^0(1+\alpha)} = \int_0^\infty dy \frac{\phi_a}{\sqrt{y\bar{n}}}\left[\phi_a\left(1 - \sqrt{\frac{y}{\bar{n}}}\right)\theta(y-\bar{n}) + \phi_b\right]^\alpha \times \left[\frac{1}{2} - \frac{1}{2}\mathrm{erf}\left(\frac{y-\bar{n}}{\sqrt{2}\Delta}\right) - \theta(y-\bar{n})\right] e^{-t/\tau(y)} \quad \text{(B52)}$$

This result is used in the calculation of the H-polymer spectra in Figure 12.

References and Notes

(1) For a recent review, see: Watanabe, H. *Prog. Polym. Sci.* **1999**, *24*, 1253.
(2) de Gennes, P.-G. *Scaling Concepts in Polymer Physics*; Cornell University Press: Ithaca, NY, 1979.
(3) Doi, M.; Edwards, S. F. *The Theory of Polymer Dynamics*; Clarendon Press: Oxford, 1986.
(4) Ball, R. C.; McLeish, T. C. B. *Macromolecules* **1989**, *22*, 1911.
(5) Milner, S. T.; McLeish, T. C. B. *Macromolecules* **1997**, *30*, 2159.
(6) Milner, S. T.; McLeish, T. C. B. *Macromolecules* **1998**, *31*, 7479.
(7) Milner, S. T.; McLeish, T. C. B. *Phys. Rev. Lett.* **1998**, *81*, 725.
(8) Blottière, B.; McLeish, T. C. B.; Hakiki, A.; Young, R. N.; Milner, S. T. *Macromolecules* **1998**, *31*, 9295.
(9) Milner, S. T.; McLeish, T. C. B.; Young, R. N.; Hakiki, A.; Johnson, J. M. *Macromolecules* **1998**, *31*, 9345.
(10) McLeish, T. C. B.; Allgaier, J.; Bick, D. K.; Bishko, G.; Biswas, P.; Blackwell, R.; Blottiére, B.; Clarke, N.; Gibbs, B.; Groves, D. J.; Hakiki, A.; Heenan, R. K.; Johnson, J. M.; Kant, R.; Read, D. J.; Young, R. N. *Macromolecules* **1999**, *32*, 6734.
(11) Daniels, D. R.; McLeish, T. C. B.; Crosby, B. J.; Young, R. N.; Fernyhough, C. M. *Macromolecules* **2001**, *34*, 7025.
(12) Gell, C. B.; Graessley, W. W.; Efstratiadis, V.; Pitsikalis, M.; Hadjichristidis, N. *J. Polym. Sci. B* **1997**, *35*, 1943.
(13) Jordan, E. A.; Donald, A. M.; Fetters, L. J.; Klein, J. *ACS Polym. Prepr.* **1989**, *30*, 63.
(14) Pearson, D. S.; Helfand, E. *Macromolecules* **1984**, *17*, 888.
(15) Colby, R. H.; Rubinstein, M. *Macromolecules* **1990**, *23*, 2753.
(16) Frischknecht, A. L.; Milner, S. T. *Macromolecules* **2000**, *33*, 9764.
(17) Morton, M.; Fetters L. J. *Rubber Chem. Technol.* **1975**, *48* (3), 359. Iatrou, H.; Hadjichristidis, N. *Macromolecules* **1992**, *25*, 4649.
(18) Tanaka, Y.; Takeuchi, Y.; Kobayashi, M.; Tadokoro, H. *J. Polym. Sci., Part A-2* **1971**, *9*, 43.
(19) Gotro, J. T.; Graessley, W. W. *Macromolecules* **1984**, *17*, 2767.
(20) Fetters, L. J.; Lohse, D. J.; Richter, D.; Witten, T. A.; Zirkel, A. *Macromolecules* **1994**, *27*, 4639.
(21) Ferry, J. D. *Viscoelastic Properties of Polymers*; Wiley: New York, 1980; p 330.
(22) The value of p^2 used in ref 10 was incorrectly reported to be $p^2 = 1/6$; in fact, a value of $p^2 = 1/12$ was used in Figures 6(a)−6(c) of that reference, with the exception of the dashed curves in Figure 6, parts a and c, which do correspond to $p^2 = 1/6$. Thus, the effect of the polydispersity correction is overestimated in Figure 6, parts a and c of ref 10. Nevertheless, using our calculations for the effects of polydispersity, we find a value of $p^2 = 1/6$ actually fits the H-polymer data from ref 10 (see section 4 and Figure 12).
(23) Likhtman, Alexei. Private communication.
(24) The result for $\tau(s)$ in eq 19 of ref 5 is mistakenly smaller than it should be by a factor of 2, although the factors are correct in eq 29 of ref 5. The same factor of 2 is also missing in eq 10 of ref 6 (despite the parenthetical note to the contrary) and in eqs 30 and 39 of ref 10. The correct expression for $\tau(s)$ was used in the calculations of ref 7.

MA0101411